Investigations of Evanescent Wave Optical Sensors using Beam Propagation Method

A Thesis Submitted

in Partial Fulfillment of the Requirements

for the Degree of

Master of Technology

by

VINAY KUMAR

to the

Laser Technology Programme,

Indian Institute of Technology Kanpur

June, 2005

TH
LT/2005/M
K96l

13 JUL 2005/LT
सतीश कामीनाथ केलकर पुस्तकालय
भारतीय प्रौद्योगिकी संस्थान कानपुर
वर्गाप्ति क्र० A... 152057



CERTIFICATE

This is to certify that the work contained in the thesis entitled "**Investigations of Evanescent Wave Optical Sensors using Beam Propagation Method**", by **Vinay Kumar (Roll No Y3116010)**, has been carried out under my supervision and this work has not been submitted elsewhere for a degree.

Dr. Joseph John,
Professor,
Center for Laser Technology
Indian Institute of Technology Kanpur
Kanpur – 208016

Dr. Anjan Kumar Ghosh
Professor,
Center for Laser Technology
Indian Institute of Technology Kanpur
Kanpur – 208016

June 2, 2005

POST GRADUATE OFFICE
THESIS SUBMITTED ON 5/6/05
I.I.T., KANPUR-200 016

ABSTRACT

The need of telecommunications continue to increase and new methods of utilizing more of the potential bandwidth through optical fiber become more popular. So the demands placed on light wave systems have dramatically increased, spurring development of light wave.components. So the demand of modeling of optoelectronics devices has increased the importance of numerical methods in sharp manner. Beam Propagation Method is an very efficient tool to analyze the propagation of wave through the complex structure.

In this Thesis Finite Difference Beam Propagation Method is used to analysis the slab wave guide. Slowly varying envelope Approximation is used which help the method to choose the relatively bigger step size, lesser memory space, lesser computational time as compared to other numerical technique. Transparent Boundary Condition is also used because of limited computational window. Analysis of perturbed Slab wave guide structure is done. Effect of cladding removal and effect of different Refractive Index at the substrate in slab wave guide structure is also analyzed.

Dedicated

to

My Parents

ACKNOWLEDGEMENTS

I am indebted my thesis supervisor Dr. Joseph John and Dr. Anjan K. Ghosh for their inspiring guidance and constant encouragement throughout the progress of my work. I benefited a lot from the discussions I had with them from time to time and I feel privileged that I am able to harness something from his vast experience in the field of "Optical Sensors". I wish to express my deep sense of gratitude to them for his valuable suggestions and incomparable help. It was due to there supportive nature and supervision that I could work in this field successfully.

I am thankful to Mr. Sivabalan for the valuable discussions and the unselfish helps rendered from time to time in spite of a busy schedule in this campus. Putting down a few words of thanksgiving would not justify the wholehearted support that I received from him.

I am especially grateful to my colleagues and friends, Manish, Ajay, Manisha, Neha, Rajesh, Dilip and Smitha , for their excellent company and support during my work. I would also like to thank all my classmates whose company made my stay at IIT Kanpur a memorable experience.

Last but not the least, I express my special gratitude to my parents for their love, support and encouragement and for boosting my morale in hard times.

Vinay Kumar

CONTENTS

	Page No
List of Figures	ix
List of Tables	xii
List of Symbols	xiii
CHAPTER 1	
INTRODUCTION	1
1.1 Thesis objective	1
1.2 Beam Propagation Method (BPM)	3
1.3 Thesis Organization	4
CHAPTER 2	
FINITE DIFFERENCE BEAM PROPAGATION METHOD THEORY AND ITS IMPLEMENTATION	5
2.1 Finite Difference Beam Propagation Method Principles	5
2.2 Derivation of the FD-BPM Algorithm	7
2.2.1 Maxwell's Equations	7
2.2.2 The Wave Equation	7
2.2.3 FDBPM Formulation	10
2.3 Finite Difference Method	11
2.3.1 Taylor Series Expansion	11
2.3.2 First Derivative	11
2.3.3 Second Derivatives	12
2.3.4 Numerical Application of finite difference Method	13
2.4 Selection of n_{eff}	16
2.5 Transparent Boundary Condition	17
2.5.1 Left hand boundary:	17

2.5.1 Left hand boundary: 17
2.5.2 Right Hand Boundary 19
2.6 Numerical Application Of TBC 20
2.6.1 Left Hand Boundary (p=1) 21
2.6.2 Right Hand Boundary (p=M) 22

CHAPTER 3

ACCURACY OF THE SOFTWARE 24
3.1 Laser Beam Propagation 24
3.1.1 FWHM calculation by FRESNEL equation for Gaussian propagation 32
3.2 FWHM calculation by FDBPM 32
3.3 Error in FWHM measured by FDBPM 34
3.4 Mode Calculation Theory 35
3.5.Varification for the result for Wave guide 36

CHAPTER 4

RESULT AND DISCUSSIONS 39
4.1 Free Space Propagation 39
4.1.1 FDBPM without Boundary Condition 39
4.1.2 FDBPM with Boundary Condition 40
4.2 Single mode and Multimode Structure Analyses 41
4.3 Power Calculation 44
4.3.1 Trapezoidal Method 45
4.3.2 Simpson's Rule 46
4.4 Refractive Index Sensing with Evanescent Field 48
4.4.1 Mathematical Analysis of Evanescent Wave Sensor 48
4.4.2 Sensitivity of the Sensor 49
4.4.3 Factors affecting Sensitivity 50
4.5 Analysis of Perturbation in Slab Waveguide 50
4.5.1 Effect of Cladding Removal 52
4.5.2 Effect of Refractive Index on Output Power 53
4.6 Optical Sensor 55

4.6 Optical Sensor 55
4.7 Effect of Strip 59
4.8 Effect of Roughness in clad Removal 61

CHAPTER 5

CONCLUSIONS AND SUGGESTIONS FOR FUTURE WORK 64

5.1 Suggestions for future work 65

References 66

LIST OF FIGURES

		Page No
Figure 1.1	Structure Of Slab Waveguide(3d view)	3
Figure 2.1	Slab waveguide structure analyzed in the thesis	5
Figure 2.2	The BPM algorithm calculates the next field from present field	6
Figure 2.3	Three Layer Slab Waveguide Structure	8
Figure 2.4	Discretization of Computational Window	14
Figure 2.5	ω-β curve	16
Figure 2.6	Nodes at p=0 and p=M+1 are outside the analyses window	17
Figure 3.1	The normalized beam intensityI/I_0 as a function of the radial distance ρ at different axial distances: (a) z = 0 (b) z = z_0 (c) z = $2z_0$	28
Figure 3.2	The normalized beam intensity I/I_0 at points on the beam axis (ρ = 0) as a function of z	29
Figure 3.3	Beam radius as a function of propagation distance	30
Figure 3.4	The depth of focus of a Gaussian beam	31
Figure 3.5	Phase retardation of the Gaussian beam relative to a uniform planewave at points on the beam axis	32
Figure 3.6	Free space Propagation of Gaussian Wave	33
Figure 3.7	FWHM calculated by FDBPM and FRESNEL calculation	33
Figure 3.8	Error in FWHM by Fresnel equation and FWHM by FDBPM	34
Figure 3.9	Slab Waveguide Structure	35
Figure 3.10	Amplitude Profile of Slab wave guide structure by calculation	37
Figure 3.11	Amplitude Profile of Slab wave guide structure by FDBPM	37
Figure 4.1	Intensity profile without boundary condition	40
Figure 4.2	Intensity profile with boundary condition	40

Figure 4.3	Intensity profile at 400um	41
Figure 4.4	Slab wave Guide Structure (5 layer)	41
Figure 4.5	Single Mode Intensity profile	42
Figure 4.6	Half of the Intensity Profile At Out Put	42
Figure 4.7	Top view of the intensity profile using multimode structure	43
Figure 4.8	Intensity Profile of single mode and multimode structure	44
Figure 4.9	Trapezoid area calculation for two points	45
Figure 4.10	Trapezoid area calculation for more points	46
Figure 4.11	Total electric field of the frustrated total reflection process in TE-mode. On the right, the profile in the z-direction is plotted.	48
Figure 4.12	Slab wave guide Structure With Cross Sectional Cut(3d view)	51
Figure 4.13	Slab wave guide Structure With Cross Sectional Cut (top view)	51
Figure 4.14	Intensity Profile for 70 Percentage of cut in clad	52
Figure 4.15	Intensity Profile for different Percentage of cut in clad	53
Figure 4.16	Effect of Refractive index (less than core) on the output power for different percentage of clad removed structure	54
Figure 4.17	Effect of Refractive index on the output power for different percentage of clad removed structure	54
Figure 4.18	Structure Of Proposed Optical Sensor	56
Figure 4.19	Intensity Profile for Surrounding Refractive Index at 1.44	56
Figure 4.20	Intensity Profile for Surrounding Refractive Index at 1.44	57
Figure 4.21	Intensity Profile for Surrounding Refractive Index at 1.50	57
Figure 4.22	Intensity Profile for Surrounding Refractive Index at 1.50	58
Figure 4.23	Effect of Refractive Index on Output Power	58

Figure 4.24 Structure with 1um strip on both side of core 59

Figure 4.25 Effect of Strip on Output Power with Surrounding Refractive Index 60

Figure 4.26 Waveguide structure with roughness due to clad removal 61

Figure 4.27 Effect of Roughness and Refractive Index on Output Power 62

LIST OF TABLES

		Page No.
Table 3.1	:Error in FWHM measured by FDBPM	6
Table 4.1	: Change in Output Power for Different percentage of clad Removal(Surrounding Medium Refractive Index=1.00)	7
Table 4.2	: Effect of strip Refractive Index on Output Power	17
Table 4.3	: Effect of Roughness and Refractive Index on Output Power	62

LIST OF SYMBOLS

ε_r	Relativity Permittivity
μ_r	Relativity Permeability
n	Refractive Index
β	Propagation Constant
n_{eff}	Effective Refractive Index
k_0	Wave Number in free space
λ_0	Wavelength in free space
Φ_p^l	Wave function at p^{th} step in x direction and l^{th} step in z direction
$\varepsilon_r^l(p)$	Relativity Permeability at p^{th} step in x direction and l^{th} step in z direction
k_x	Wave number in x direction
Δz	Z step
Δx	X step
W_0	Beam Waist
$W(z)$	Beam width at distance z
$\xi(z)$	Phase Retardation
V	Normalized Frequency
θ_c	Critical angle

Chapter 1

INTRODUCTION

1.1 Introduction

The use and requirement of telecommunication continues to increase and new methods, utilizing most of the potential bandwidth through optical fiber is becoming more popular. The demands placed on light wave systems have dramatically increased, spurring development of light wave components such as fibers, lasers, detectors, modulators, switches, and wavelength multiplexing/demultiplexing devices.

The analysis of theses devices is useful for the development of optical communication. Nowadays many types of analysis of such components exist: Exact Analytical, Numerical and Semi-Analytical methods. Exact analytical methods are heavily restricted to only very simple slab devices, limiting their use in the analysis of complex 3D structures. Consequently, in the quest for analysis, more attention has been focused on Numerical and approximate Semi-Analytical methods.

1.2 Beam Propagation Method (BPM)

Among the different numerical techniques developed for modeling guided-wave propagation in integrated optics and fiber optics, the most popular is the beam propagation method (BPM)[1][2]. Unlike the finite-difference time-domain (FDTD) technique and finite element Method (FEM), which simulates the device's performance through a rigorous numerical solution of Maxwell's equations, the BPM takes advantage of some simplifications common to many problems.

The simplifications offered by the BPM reduce the computational complexity of most problems, speeding up the computational process for many problems, and in some cases making otherwise impossible computations realistically solvable. By eliminating the second derivative term in *z*, the problem of solving Helmholtz equation is reduced from a second-order boundary value problem requiring iteration or eigenvalue analysis to a first-order initial-value problem that can be solved by simple "integration" along the propagation direction z.

Numerical methods such as FTDT or FEM sometimes require large amounts of memory and computational resources. Consequently, in certain situations, it is extremely difficult to apply numerical methods, especially where the structure is large and complex (such as the array waveguide structures). In these cases, a Semi-Analytical method [3], such as the Effective Index (EI) method [4], Spectral Index (SI) method [5], or Free Space Radiation Mode (FSRM) method [6] may be chosen for analysis, depending on the geometry. Each method uses approximations to reduce the complexity of the device, which can result in a fast application suitable for design purposes, with the additional advantages of much lower requirements in CPU time and resources.

In this thesis research numerical method, Finite Difference Beam Propagation (FDBPM), is used for the analysis and design of evanescent wave based guided wave optical devices for the measurement of refractive index of the liquids. Propagation of monochromatic wave in slab waveguide structure is studied. Here 2D Waveguide structure is used for the analysis of the effect of refractive index. The Structure of waveguide is as shown in figure 1.1.

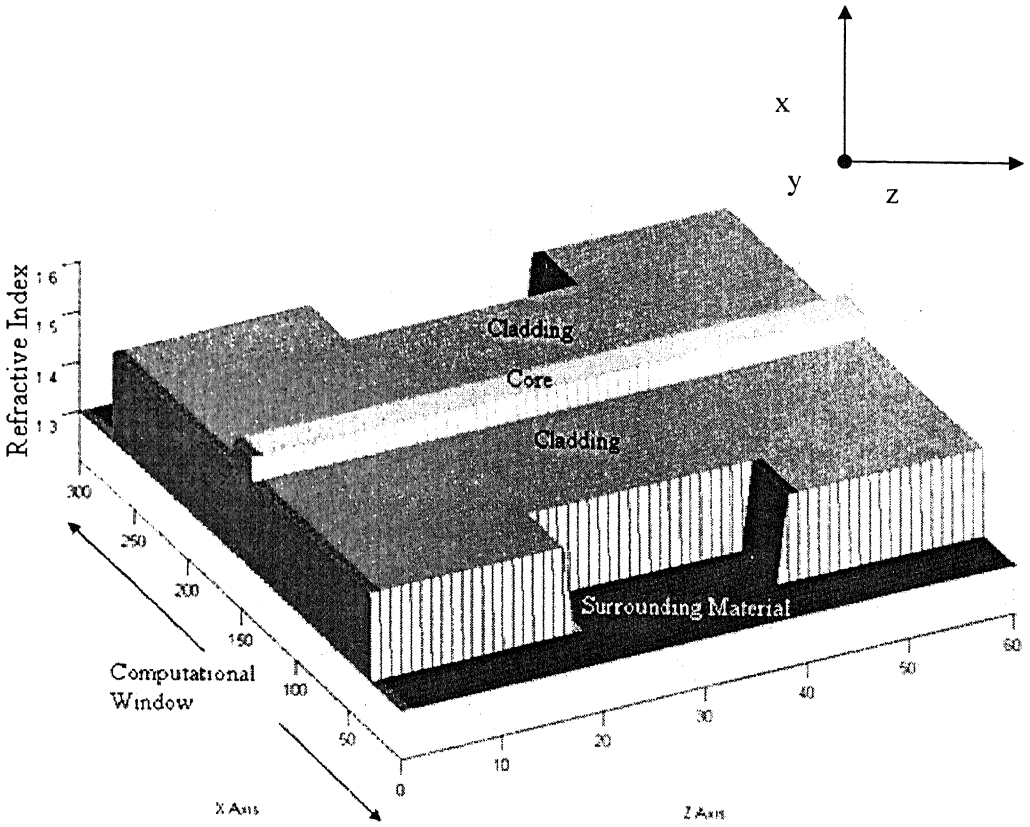


Figure 1.1 Structure of Slab waveguide

In this Thesis research the output power is measured with change in refractive index of the Surrounding medium as well as change in different amount of the cut in the cladding. Effect of concentration of sucrose solution on the output power is also analyzed. Effect of perturbation and strips on core is also studied.

1.3 Thesis Organization

Chapter 2 describes the theory of BPM and FDBPM. In this chapter mathematical model of finite difference method, Transparent Boundary Condition will be discussed and applied into numerical method.

Chapter 3 deals with the accuracy and validation of simulation program.

Chapter 4 discusses the effect of different percentage of cross sectional cut in the slab waveguide structure. In this chapter we also see the effect of change of refractive index at the surrounding medium of slab is also discussed.

Chapter 5 concludes the thesis with the major results and gives suggestions for further work in this area

Chapter 2

FINITE DIFFERENCE BEAM PROPAGATION METHOD THEROY AND ITS IMPLIMENTATION

In this chapter, the basic concepts of Finite Difference Beam Propagation Method (FD-BPM) [7] is discussed and its algorithm is derived. This derivation is based on the Maxwell' Wave Equations [8][9], vector wave equation, and its the Scalar form is derived. The finite difference method is used with Crank-Nicholson (CN) propagation scheme [10], known for its accuracy and stability, to solve the scalar form of wave equation. Transparent Boundary condition [11] is applied to reduce the effect of the simulation space limits on the solution, such that it can be used for a real time application. Methods of implementation into a computer program are explored with the aim of making a set of reliable and efficient solvers that are suitable for the simulation of large components.

2.1 Finite Difference Beam Propagation Method Principles.

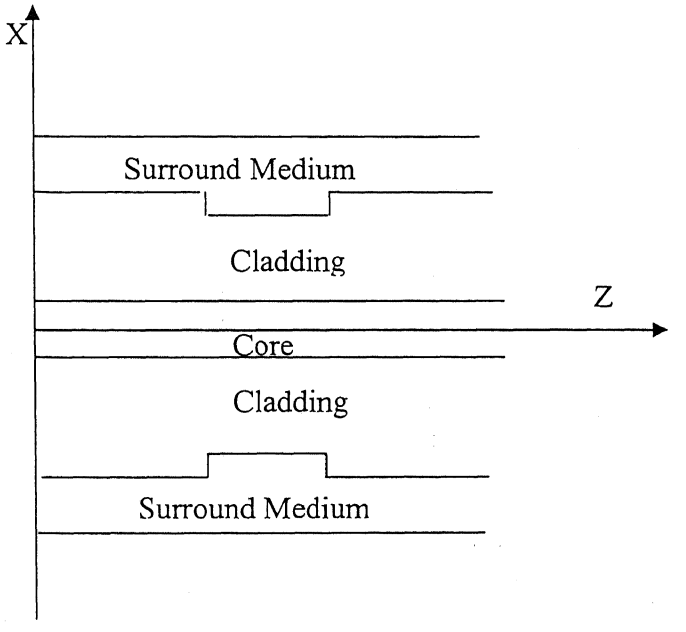


Figure 2.1 Slab Waveguide structure used for thesis

The Finite Difference – Beam Propagation Method (FD-BPM) [7] is a popular numerical algorithms used to determine light propagation in the physical structures like slab waveguide (Figure 2.1.)[12][13]. It is a used to solve the Maxwell's Wave Equations and it can be applied to complex waveguide structures. A good commercial example of BPM software package is BeamProp by RSoft Design Group, Inc. [14]. The FD-BPM samples both the structure and field in analysis. The structure was uniformly sampled in steps of Δz in the direction of propagation of the wave and the field was also uniformly sampled in steps of Δx in the transverse direction of propagation of wave. Figure 2.2 demonstrate the FD-BPM working in the 2D case. From a known set of 'present' points, forming a line in 2D implementations as shown in figure 2.2, the field at the 'next' set of points is calculated. Knowledge of the structure at all points is required. This process is repeated for each new set of known field points, and so the simulation 'propagates' in the z-direction.

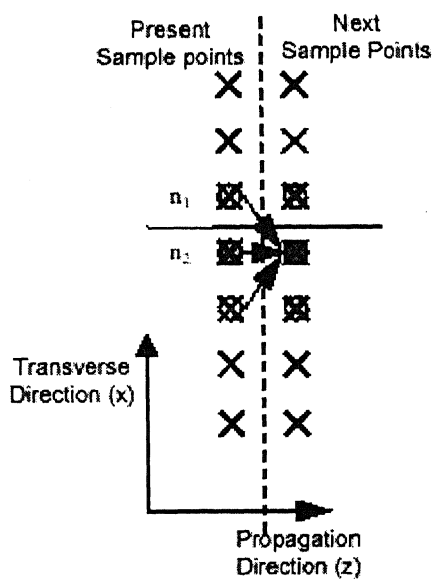


Figure 2.2 The BPM algorithm calculates the 'next' field from the 'present' field.

2.2 Derivation of the FD-BPM Algorithm

2.2.1 Maxwell's Equations

The following Maxwell's wave equation are solved by using Finite Difference – Beam Propagation Method (FD-BPM) [7]. In a source free region, and assuming a periodic time variation, $e^{j\omega t}$ they are:

$$\Delta \times \bar{E} = -j\mu\omega\bar{H} \tag{2.1}$$

$$\Delta \times \bar{H} = j\mu\omega\bar{E} \tag{2.2}$$

$$\Delta \bullet \varepsilon\bar{E} = 0 \tag{2.3}$$

$$\Delta \bullet \mu\bar{H} = 0 \tag{2.4}$$

where $\varepsilon = \varepsilon_r\varepsilon_0$ and $\mu = \mu_0\mu_r$, and the vector quantity E (V/m) is the electric field vector and H (A/m) is the magnetic field vector and a periodic time variation $e^{j\omega t}$ has been assumed. The quantities ε and μ define the electromagnetic properties of the medium. $\varepsilon_0 = 8.854\times10^{-12}$ Fm^{-2} is the dielectric constant in vacuum and $\mu_0 = 4\ \pi\ \times10^{-7}$ Hm^{-2} is the magnetic permeability in a vacuum. ε_r and μ_r are there relative permittivity and permeability of the material. In this work μ_r has unity value since only non-magnetic materials are considered. ε_r had the different value depending on the type of different surrounding material used in the analysis. Using ε_r and μ_r the refractive index n, of the medium is defined as $n = \sqrt{\mu_r\varepsilon_r}$.

2.2.2 The Wave Equation

The total electromagnetic field that is supported by a waveguide can be expressed in terms of only the electric or magnetic field components to produce wave equations. Throughout this section our calculation considers only the electric field, rather than

the magnetic field. This was done by taking the curl of equation (2.1) and substituting in (2.2), i.e.

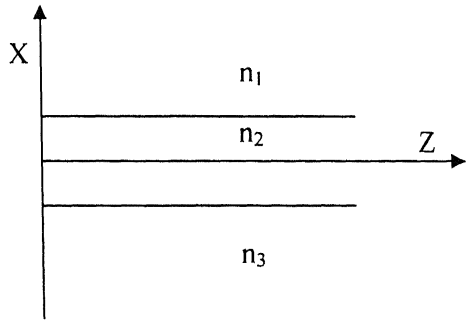


Figure 2.3 Three Layer Slab Waveguide Structure

Since structure is uniform in y direction so $\frac{\partial}{\partial y} = 0$

Equation(2.1) can be written as

$$-\frac{\partial E_y}{\partial z} = -j\omega\mu_o H_x \tag{2.5}$$

$$\frac{\partial E_x}{\partial z} - \frac{\partial E_z}{\partial x} = -j\omega\mu_o H_y \tag{2.6}$$

$$\frac{\partial E_y}{\partial x} = -j\omega\mu_o H_z \tag{2.7}$$

Equation 2.2 can be written as

$$-\frac{\partial H_y}{\partial z} = j\omega\varepsilon_o\varepsilon_r E_x \tag{2.8}$$

$$\frac{\partial H_x}{\partial z} - \frac{\partial H_z}{\partial x} = j\omega\varepsilon_o\varepsilon_r E_y \tag{2.9}$$

$$-\frac{\partial H_y}{\partial x} = j\omega\varepsilon_o\varepsilon_r E_z \tag{2.10}$$

For TE Mode ($E_x = E_z = H_y = 0$)

Substituting value of E_x, E_z, H_y in equation(2.5), equation(2.6), equation(2.7), equation(2.8) and equation(2.9)

$$-\frac{\partial E_y}{\partial z} = -j\omega\mu_o H_x \tag{2.11}$$

$$\frac{\partial E_y}{\partial x} = -j\omega\mu_o H_z \tag{2.12}$$

$$\frac{\partial H_x}{\partial z} - \frac{\partial H_z}{\partial x} = j\omega\varepsilon_o\varepsilon_r E_y \tag{2.13}$$

Putting the value of H_x from equation(2.11) and the value of H_z from equation(2.12) in equation(2.13)

$$\frac{\partial^2 E_y}{\partial z^2} + \frac{\partial^2 E_y}{\partial x^2} + \omega_o^2 \varepsilon_o \mu_o E_y = 0 \tag{2.14}$$

TM Mode ($H_x = H_z = E_y = 0$)

Substituting value of H_x, H_z, E_y in equation(2.5), equation(2.6), equation(2.7), equation(2.8) and equation(2.9)

$$\frac{\partial E_x}{\partial z} - \frac{\partial E_y}{\partial x} = -j\omega\mu_o H_y \tag{2.15}$$

$$-\frac{\partial H_y}{\partial z} = j\omega\varepsilon_o\varepsilon_r E_x \tag{2.16}$$

$$\frac{\partial H_y}{\partial x} = j\omega\varepsilon_o\varepsilon_r E_z \tag{2.17}$$

Putting the value of Ex from equation (2.16) and the value of E_z from equation (2.17) in equation (2.15) we gets

$$\frac{\partial^2 E_x}{\partial z^2} + \frac{\partial}{\partial x}\left(\frac{1}{\varepsilon_r}\frac{\partial}{\partial x}(\varepsilon_r E_x)\right) + k_o^2 \varepsilon_r E_x = 0 \tag{2.18}$$

Where k_0 is wave number in free space, λo is wavelength in free space.

$$k_0 = \frac{2\pi}{\lambda_0} \tag{2.19}$$

2.2.3 FD-BPM Formulation

The uniform sampling discussed previously is used to solve second order differential equation (equation 2.14).

$$\frac{\partial^2 E_y}{\partial z^2}+\frac{\partial^2 E_y}{\partial x^2}+\omega_o{}^2\varepsilon_o\mu_o E_y=0$$

Assuming the solution of equation (2.14) is as follows

$$E_y(x,y,z)=\Phi(x,y,z)\exp(-j\beta z) \tag{2.20}$$

Slowly envelope approximation is used to separate E_y into slowly varying envelope function $\Phi(x,y,z)$ and fast oscillating phase term $\exp(-j\beta z)$. β is propagation constant in z direction. β and k_0 are related as follows.

$$\beta = n_{eff}\times k_0 \tag{2.21}$$

where n_{eff} is refractive index.

Putting the value of E_y in equation (2.14) we get

$$\frac{\partial^2\Phi}{\partial z^2}-2j\beta z\frac{\partial\Phi}{\partial z}-\beta^2\Phi+\frac{\partial^2\Phi}{\partial x^2}+k_o{}^2\varepsilon_r\Phi=0 \tag{2.22}$$

As $\Phi(x,y,z)$ is a slowly varying envelope function in z direction

$$\frac{\partial\Phi}{\partial z}\gg\frac{\partial^2\Phi}{\partial z^2} \tag{2.23}$$

So
$$\frac{\partial^2\Phi}{\partial z^2}\simeq 0 \tag{2.24}$$

Using this equation (2.22) becomes

$$\frac{\partial^2\Phi}{\partial x^2}-2j\beta z\frac{\partial\Phi}{\partial z}-\beta^2\Phi+k_0{}^2\varepsilon_r\Phi=0 \tag{2.25}$$

2.3 Finite Difference Method:-

Finite difference method is an idea of approximating the derivatives of a continuous function by dividing up the function into segments and looking at how the slope (first derivative) varies between segments. Consider a function $u(x)$, divided along the x-axis into segments of width Δx. Consider one grid point (segment boundary) near the center at grid point at position x given by x_j. The point to the left at x-Δx is grid point x_{j-1} and the point to the right is at $x+\Delta x$ is at grid point x_{j+1}. We can extract information about the first and second derivative of the function $u(x)$ from the information and grid points by using the following technique.

2.3.1 Taylor Series Expansion

The Taylor series expansion relates the value of the function $u(x)$ to values at adjacent points ($x+\Delta x$ or x-Δx) and the derivatives of $u(x)$. For example:

$$u(x+\Delta x) = u(x) + \Delta x \frac{\partial u}{\partial x} + \frac{\Delta x^2}{2}\frac{\partial^2 u}{\partial x^2} + \frac{\Delta x^3}{6}\frac{\partial^3 u}{\partial x^3} + \qquad (2.26)$$

and

$$u(x-\Delta x) = u(x) - \Delta x \frac{\partial u}{\partial x} + \frac{\Delta x^2}{2}\frac{\partial^2 u}{\partial x^2} - \frac{\Delta x^3}{6}\frac{\partial^3 u}{\partial x^3} + \qquad (2.27)$$

Thses equations are used to determine the first order and second order derivative in the following section.

2.3.2 First Derivatives ($\frac{\partial u}{\partial x}$)

Forward Difference

If we keep only the first two terms of the expansion for $u(x+\Delta x)$, then

$$\frac{\partial u}{\partial x} = \frac{u(x+\Delta x) - u(x)}{\Delta x} \qquad (2.28)$$

This is a first order accurate solution (O (Δx)). It is called the forward difference since it finds the derivative in the positive (forward) direction of the profile from the point at x.

Backward Difference

Considering only the first two terms of the expansion for $u(x\text{-}\Delta x)$, in equation (2.27)

$$\frac{\partial u}{\partial x} = \frac{u(x) - u(x + \Delta x)}{\Delta x} \tag{2.29}$$

This is a first order accurate solution ($O(\Delta x)$). It is called the backward difference since it finds the derivative in the negative (backward) direction of the profile from the point at x.

Centered Difference

To get a more accurate representation of the first derivative, find the difference between $u(x+\Delta x)$ and $u(x\text{-}\Delta x)$ is combined using equation (2.26) and equation (2.27) we get

$$u(x + \Delta x) - u(x - \Delta x) = u(x) + \Delta x \frac{\partial u}{\partial x} + \frac{\Delta x^2}{2} \frac{\partial^2 u}{\partial x^2} - u(x) + \Delta x \frac{\partial u}{\partial x} - \frac{\Delta x^2}{2} \frac{\partial^2 u}{\partial x^2} \tag{2.30}$$

On simplification we get the following equation.

$$\frac{\partial u}{\partial x} = \frac{u(x + \Delta x) - u(x - \Delta x)}{2\Delta x} \tag{2.31}$$

This is a second order accurate solution (here the Δx^2 terms is included, they just happen to cancel out - $O(\Delta x^2)$). It is called a centered difference, because it is centered at the position x, but uses information from both adjacent points.

2.3.3 Second Derivative ($\frac{\partial^2 u}{\partial x^2}$)

For the differential equation, we actually need the second derivative. Using the Taylor series expansion, the sum of $u(x+\Delta x)$, form equation (2.26) and, $u(x\text{-}\Delta x)$ form equation (2.27) we get

$$u(x+\Delta x)+u(x-\Delta x)=u(x)+\Delta x\frac{\partial u}{\partial x}+\frac{\Delta x^2}{2}\frac{\partial^2 u}{\partial x^2}+u(x)-\Delta x\frac{\partial u}{\partial x}+\frac{\Delta x^2}{2}\frac{\partial^2 u}{\partial x^2} \quad (2.32)$$

On simplification we get

$$u(x+\Delta x)+u(x-\Delta x)=2u(x)+\Delta x^2\frac{\partial^2 u}{\partial x^2} \quad (2.33)$$

Solving for $\frac{\partial^2 u}{\partial x^2}$

$$\frac{\partial^2 u}{\partial x^2}=\frac{u(x+\Delta x)+u(x-\Delta x)-2u(x)}{\Delta x^2} \quad (2.34)$$

This is again a centered difference, but it also uses information about u(x) at position x. It is also second order accurate($O(\Delta x^2)$).

The accuracy can be improved by decreasing Δx. This is the easiest and fastest way to improve accuracy, but it comes with a computational cost and taking more time and memory.

2.3.4 Numerical application of finite difference method

Again using equation (2.25)

$$2j\beta z\frac{\partial \Phi}{\partial z}=\frac{\partial^2 \Phi}{\partial x^2}-\beta^2\Phi+k_0^2\varepsilon_r\Phi \quad (2.35)$$

Using discretization in x and z direction we get

$$x = p\,\Delta x \quad (2.36)$$

$$z = l\,\Delta z \quad (2.37)$$

p, l are integers. Δz and Δx are uniform small steps in the direction of propagation and transverse to the direction of propagation respectively. Figure 2.4 shows the discretization scheme on the computational window

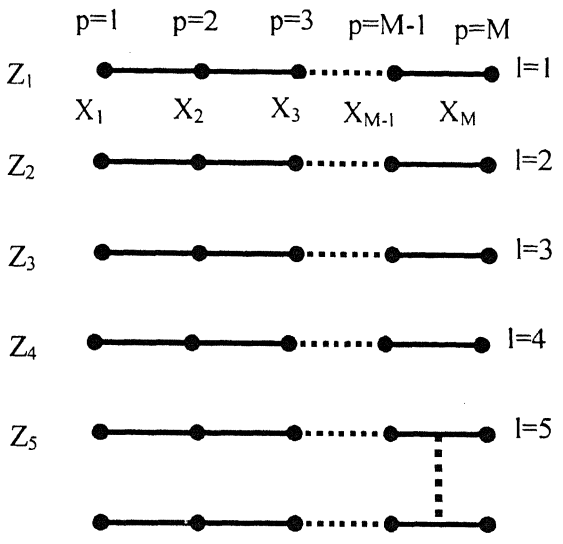


Figure 2.4 Discretization in the computational window

following notations are used for wave function $\Phi(x,z)$ and relative permittivity $\varepsilon_r(x,z)$.

$$\Phi(x,z) = \Phi^{l}{}_{p} \tag{2.38}$$

$$\varepsilon_r(x,z) = \varepsilon_r{}^{l}(p) \tag{2.39}$$

Using this in equation (2.34) we get the discretization in the z direction as follows

$$\frac{\partial^2\Phi}{\partial x^2} = \frac{1}{\Delta x}\left(\frac{\Phi_{p+1}-\Phi_p}{\Delta x} - \frac{\Phi_p-\Phi_{p-1}}{\Delta x}\right) \tag{2.40}$$

$\frac{\Phi_{p+1}-\Phi_p}{\Delta x}$ has centre difference at p+1/2

$\frac{\Phi_p-\Phi_{p-1}}{\Delta x}$ has centre difference at p-1/2

$$\frac{\partial^2\Phi}{\partial x^2} = \left(\frac{\Phi_{p+1}-2\Phi_p+\Phi_{p-1}}{\Delta x^2}\right) \tag{2.41}$$

Equation (2.41) has centre difference at point p

$$k_0{}^2(\varepsilon_r - n_{eff}{}^2)\Phi = k_0{}^2(\varepsilon_r(p) - n_{eff}{}^2)\Phi_p \tag{2.42}$$

Equation (2.42) has centre difference at point p

Putting the values in equation(2.35) form equation(2.40) and equation(2.42) we get

$$2j\beta\frac{\partial\Phi}{\partial z}=(\frac{\Phi^{l}_{p+1}-2\Phi^{l}_{p}+\Phi^{l}_{p-1}}{\Delta x^2})+k_0{}^2(\varepsilon_r{}^{l}(p)-n_{eff}{}^2)\Phi^{l}_{p} \qquad (2.43)$$

Now discretizing the equation (2.35) in z direction.

$$2j\beta\frac{\partial\Phi_p}{\partial z}=2j\beta(\frac{\Phi^{l+1}_{p}-\Phi^{l}_{p}}{\Delta z}) \qquad (2.44)$$

Discretizing centre of left hand side of equation (2.44) is at l+1/2 while right hand side of equation (2.35) has discretizing centre at l.

Now using Crank Nicholson (CN) scheme to get the solution of equation (2.35) at the same discretizing centre with good stability. If we have field profile at z and at $z+\Delta z$ then its discretization center will be at $z+\Delta z/2$. Crank Nicholson (CN) scheme has proposed an difference parameter α. Which defines the α amount of field at z and (1- α) amount of field at $z+\Delta z$ are added to calculate the field at $z+\Delta z/2$. For good stability α is proposed 0.5.

So equation (2.41) will be as follows.

$$2j\beta(\frac{\Phi^{l+1}_{p}-\Phi^{l}_{p}}{\Delta z})=\frac{1}{2}\{[(\frac{\Phi^{l+1}_{p+1}-2\Phi^{l+1}_{p}+\Phi^{l+1}_{p-1}}{\Delta x^2})+k_0{}^2(\varepsilon_r{}^{l+1}(p)-n_{eff}{}^2)\Phi^{l+1}_{p}]+$$

$$[(\frac{\Phi^{l}_{p+1}-2\Phi^{l}_{p}+\Phi^{l}_{p-1}}{\Delta x^2})+k_0{}^2(\varepsilon_r{}^{l}(p)-n_{eff}{}^2)\Phi^{l}_{p}]\}$$

$$\Phi^{l+1}_{p-1}[-\frac{1}{2\Delta x^2}]+\Phi^{l+1}_{p}[-\frac{2j\beta}{\Delta z}+\frac{1}{2\Delta x^2}-\frac{k_0{}^2}{2}(\varepsilon_r{}^{l+1}(p)-n_{eff}{}^2)]+\Phi^{l+1}_{p+1}[-\frac{1}{2\Delta x^2}]=$$

$$\Phi^{l}_{p-1}[\frac{1}{2\Delta x^2}]+\Phi^{l}_{p}[\frac{2j\beta}{\Delta z}-\frac{1}{\Delta x^2}+\frac{k_0{}^2}{2}(\varepsilon_r{}^{l}(p)-n_{eff}{}^2)]+\Phi^{l}_{p+1}[\frac{1}{2\Delta x^2}] \qquad (2.45)$$

Let $\alpha_w=\frac{1}{\Delta x^2}$

$$\alpha_x=-\frac{2}{\Delta x^2}$$

$$\alpha_e = \frac{1}{\Delta x^2}$$

$$\Phi^{l+1}{}_{p-1}[-\alpha^{l+1}{}_w] + \Phi^{l+1}{}_p[\frac{4j\beta}{\Delta z} - \alpha^{l+1}{}_x - k_0{}^2(\varepsilon_r{}^{l+1}(p) - n_{eff}{}^2)] - \Phi^{l+1}{}_{p+1}[\alpha^{l+1}{}_e] =$$

$$\Phi^{l}{}_{p-1}[\alpha^{l}{}_w] + \Phi^{l}{}_p[\frac{4j\beta}{\Delta z} + \alpha^{l}{}_x + k_0{}^2(\varepsilon_r{}^{l}(p) - n_{eff}{}^2)] + \Phi^{l}{}_{p+1}[\alpha^{l}{}_e] \qquad (2.46)$$

2.4 Selection of n_{eff}

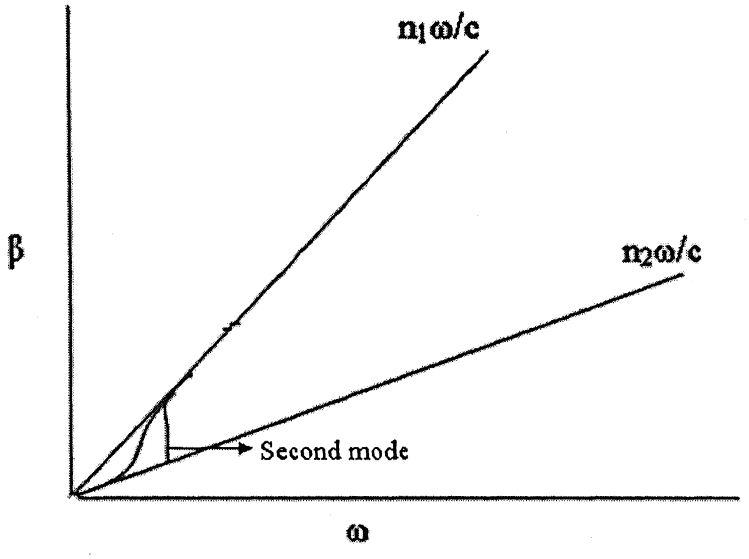


Figure 2.5 ω-β curve

In the Slab Wave structure only those mode will propagate for whom The ω/β is fix. During the analysis of slab waveguide structure the we have used the single mode structure. Single mode have no cutoff frequency. While second order mode have cutoff frequency as shown in figure 2.5. So we have taken the value of n_{eff} 5 percent of difference of core and cladding refractive index value less from the core refractive index.

2.5 Transparent Boundary Condition

An infinite wide area have no analysis boundary and there fore no reflections are coming from the boundaries. But such an area cannot be assumed in actual design, therefore, a limited analysis window is used. In actual structures, radiated waves are reflected at boundaries and return to the core area, where they interact with the propagating fields and degrades the calculation accuracy. In this section TBC is discussed which is developed by Hadley[10]. It is a way to efficiently suppress the reflection at the boundary.

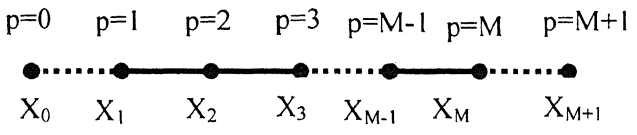


Figure 2.6 Nodes at p=0 and p=M+1 are outside the analysis window

Assuming that the analysis window (figure 2.6) contains nodes from p=1 to p=M. To analysis the effect of reflection at the computational boundaries hypothetical nodes at p=0 and p=M+1 are assumed outside the analysis window.

In the following sections Transparent Boundary Condition (TBC) is applied at the left hand boundary (p=1) and at the right hand boundary (p=M) of the analysis window

2.5.1 Left Hand Boundary:

Considering the left hand boundary in figure 2.5 we incorporate the influence of the hypothetical node at p=0(outside the analysis window) into the node at p=1(inside the analysis window) The wave function for the left traveling wave with the x-directed wave number k_x is expressed as

$$\Phi(x,z) = A(z)\exp(jk_x x) \tag{2.47}$$

Assuming that the notation for x coordinate and the fields of the nodes at p=0, 1, 2 is x_0, x_1, x_2 and Φ_0, Φ_1, Φ_2 respectively it is assumed that

$$\Phi_0(x,z) = A(z)\exp(jk_x x_0) \tag{2.48}$$

$$\Phi_1(x,z) = A(z)\exp(jk_x x_1) \tag{2.49}$$

$$\Phi_2(x,z) = A(z)\exp(jk_x x_2) \tag{2.50}$$

The field Φ_1 and Φ_2 are inside the analysis window while Φ_0 is the hypothetical field whose influence is incorporated into the field inside the analysis window.

Dividing equation (2.50) by equation(2.49) we get

$$\frac{\Phi_2}{\Phi_1} = \exp(jk_x \Delta x) \tag{2.51}$$

Dividing equation (2.49) by equation (2.48) we get

$$\frac{\Phi_1}{\Phi_0} = \exp(jk_x \Delta x) \tag{2.52}$$

Where $\Delta x = x_2 - x_1 = x_1 - x_0$

Let $$\frac{\Phi_2}{\Phi_1} = \exp(jk_x \Delta x) = \eta_1 \tag{2.53}$$

Now using equation (2.53) and equation (2.52) we get

$$\Phi_0 = \frac{\Phi_1}{\eta_1} \tag{2.54}$$

Now the value of x directed wave number is obtained from equation (2.53)

$$k_x = \frac{1}{j\Delta x}\ln(\eta_1) \tag{2.55}$$

Since wave travels leftward the real part of the x-directed wave number k_x should be negative. When it is positive, which implies reflection at the left-hand boundary, the sign should be changed from plus to minus.

$$\Phi_0 = \Phi_1 \exp(jk_x\Delta x) \tag{2.56}$$

2.5.2 Right Hand Boundary

Considering the right hand boundary in figure 2.5 we incorporate the influence of the hypothetical node at p=M+1(outside the analysis window) into the node at p=M(inside the analysis window)

The wave function for the left traveling wave with the x-directed wave number k_x is expressed as

$$\Phi(x,z) = A(z)\exp(-jk_x x) \tag{2.57}$$

Assuming that the notation for x coordinate and the fields of the nodes at p=M-1, M, M+1 is x_{M-1}, x_M, x_{M+1} and $\Phi_{M-1}, \Phi_M, \Phi_{M+1}$ respectively

It is assumed that

$$\Phi_{M-1}(x,z) = A(z)\exp(-jk_x x_{M-1}) \tag{2.58}$$

$$\Phi_M(x,z) = A(z)\exp(-jk_x x_M) \tag{2.59}$$

$$\Phi_{M+1}(x,z) = A(z)\exp(-jk_x x_{M+1}) \tag{2.60}$$

The field Φ_{M-1} and Φ_M are inside the analysis window while Φ_{M+1} is a hypothetical field whose influence should be incorporated into the field inside the analysis window.

Dividing equation (2.60) by equation(2.59) we get

$$\frac{\Phi_{M+1}}{\Phi_M} = \exp(-jk_x\Delta x) \tag{2.61}$$

Dividing equation (2.59) by equation(2.58) we get

$$\frac{\Phi_M}{\Phi_{M-1}} = \exp(-jk_x\Delta x) \tag{2.62}$$

Where $\Delta x = x_M - x_{M-1} = x_{M+1} - x_M$

Let $$\frac{\Phi_M}{\Phi_{M-1}} = \exp(-jk_x\Delta x) = \eta_M \tag{2.63}$$

Now using equation (2.61) and equation (2.63) we get

$$\Phi_{M+1} = \Phi_M \times \eta_M \tag{2.64}$$

Now the value of x directed wave number is obtained from equation (2.62)

$$k_x = \frac{1}{j\Delta x}\ln(\eta_M) \tag{2.65}$$

Since wave travels rightward the real part of the x-directed wave number k_x should be negative. When it is positive, which implies reflection at the right-hand boundary, the sign should be changed from plus to minus.

$$\Phi_{M+1} = \Phi_M \exp(-jk_x\Delta x) \tag{2.66}$$

2.6 Numerical Application of TBC

We know the field Φ^l at z and we want to know field Φ^{l+1} at $z+\Delta z$. Recalling Equation (2.46)

$$\Phi^{l+1}{}_{p-1}[-\alpha^{l+1}{}_w] + \Phi^{l+1}{}_p[\frac{4j\beta}{\Delta z} - \alpha^{l+1}{}_x - k_0{}^2(\varepsilon_r{}^{l+1}(p) - n_{eff}{}^2)] - \Phi^{l+1}{}_{p+1}[\alpha^{l+1}{}_e] =$$

$$\Phi^{l}{}_{p-1}[\alpha^{l}{}_w] + \Phi^{l}{}_p[\frac{4j\beta}{\Delta z} + \alpha^{l}{}_x + k_0{}^2(\varepsilon_r{}^{l}(p) - n_{eff}{}^2)] + \Phi^{l}{}_{p+1}[\alpha^{l}{}_e]$$

where unknown field at $z+\Delta z$ are $\Phi^{l+1}{}_{p-1}, \Phi^{l+1}{}_p, \Phi^{l+1}{}_{p+1}$ and known field at z are $\Phi^{l}{}_{p-1}, \Phi^{l}{}_p, \Phi^{l}{}_{p+1}$ let us assume known coefficients A(p), B(p), C(p), D(p), E(p), F(p) to be

$$A(p) = -\alpha^{l+1}{}_w \tag{2.67}$$

$$B(p) = \{\frac{4j\beta}{\Delta z} - \alpha^{l+1}{}_x - k_0{}^2(\varepsilon_r{}^{l+1}(p) - n_{eff}{}^2)\} \tag{2.68}$$

$$C(p) = -\alpha^{l+1}{}_e \tag{2.69}$$

$$D(p) = \alpha^{l}{}_{w} \tag{2.70}$$

$$E(p) = \alpha^{l}{}_{x} + \frac{4j\beta}{\Delta z} + k_0{}^2(\varepsilon_r{}^{l}(p) - n_{eff}{}^2) \tag{2.71}$$

$$F(p) = \alpha^{l}{}_{e} \tag{2.72}$$

Now using these equation, equation (2.45) will be

$$\Phi^{l+1}{}_{p-1}[A(p)] + \Phi^{l+1}{}_{p}[B(p)] + \Phi^{l+1}{}_{p+1}[C(p)] = \Phi^{l}{}_{p-1}D(p) + \Phi^{l}{}_{p}E(p) + \Phi^{l}{}_{p+1}F(p) \tag{2.73}$$

Where p represents the lateral position of the node

2.6.1 Left Hand Boundary (p=1)

The field Φ_1 of the node on the left hand boundary is influenced by the field Φ_0 of the hypothetical node outside the analysis window.

$$\Phi_0 = \Phi_1 * \Upsilon_L \tag{2.74}$$

Where $$\Upsilon_L = \frac{1}{\eta_1} = \frac{1}{\Phi^{l}{}_2 / \Phi^{l}{}_1} \tag{2.75}$$

Parameter Y_L is determined by the known field at x(i.e. l), Y_L is known so equation(2.73) can be reduced to

$$\Phi^{l+1}{}_1[B'(1)] + \Phi^{l+1}{}_2[C(1)] = \Phi^{l}{}_1[E'(1)] + \Phi^{l}{}_2[F(1)] \tag{2.76}$$

where

$$B'(1) = -\alpha^{l+1}{}_{w}\Upsilon_L + \{\frac{4j\beta}{\Delta z} - \alpha^{l+1}{}_{x} - k_0{}^2(\varepsilon_r{}^{l+1}(1) - n_{eff}{}^2)\} \tag{2.77}$$

$$C(1) = -\alpha^{l+1}{}_{e} \tag{2.78}$$

$$E'(1) = \alpha^{l}{}_{w} * \gamma_l + \alpha^{l}{}_{x} + \frac{4j\beta}{\Delta z} + k_0{}^2(\varepsilon_r{}^{l}(1) - n_{eff}{}^2) \tag{2.79}$$

$$F(1) = \alpha^{l}{}_{e} \tag{2.80}$$

2.6.2 Right Hand Boundary (p=M)

The field Φ_M of the node on the left hand boundary is influenced by the field Φ_{M+1} of the hypothetical node outside the analysis window.

$$\Phi_{M+1} = \Phi_M * \Upsilon_R \tag{2.81}$$

Where $$\Upsilon_R = \eta_M = \frac{1}{\Phi^l{}_M / \Phi^l{}_{M-1}} \tag{2.82}$$

Parameter Y_R is determined by the known field at x(i.e. l), Y_R is known so equation(2.73) can be reduced to

$$\Phi^{l+1}{}_{M-1}[A(M)] + \Phi^{l+1}{}_M[B'(M)] = \Phi^l{}_{M-1}[D(M)] + \Phi^l{}_M[E'(M)] \tag{2.83}$$

Where $$A(M) = -\alpha^{l+1}{}_w \tag{2.84}$$

$$B'(M) = -\alpha^{l+1}{}_w \Upsilon_R + \{\frac{4j\beta}{\Delta z} - \alpha^{l+1}{}_x - k_0{}^2(\varepsilon_r{}^{l+1}(M) - n_{eff}{}^2)\} \tag{2.85}$$

$$D(M) = \alpha^l{}_w \tag{2.86}$$

$$E'(M) = \Upsilon_R \alpha^l{}_e + \alpha^l{}_x + \frac{4j\beta}{\Delta z} + k_0{}^2(\varepsilon_r{}^l(M) - n_{eff}{}^2) \tag{2.87}$$

Rewriting equation (2.73) with constants we get the matrix form

$$\begin{bmatrix} B'(1) & C(1) & 0 & 0 & 0 \\ A(2) & B(2) & C(2) & 0 & 0 \\ 0 & A(3) & B(3) & \ddots & 0 \\ 0 & 0 & \ddots & \ddots & C(M-1) \\ 0 & 0 & 0 & A(M) & B'(M) \end{bmatrix} \times \begin{bmatrix} \Phi_1{}^{l+1} \\ \Phi_2{}^{l+1} \\ \vdots \\ \vdots \\ \Phi_M{}^{l+1} \end{bmatrix} = \begin{bmatrix} E'(1) & F(1) & 0 & 0 & 0 \\ D(2) & E(2) & F(2) & 0 & 0 \\ 0 & D(3) & E(3) & \ddots & 0 \\ 0 & 0 & \ddots & \ddots & F(M-1) \\ 0 & 0 & 0 & D(M) & E'(M) \end{bmatrix} \times \begin{bmatrix} \Phi_1{}^l \\ \Phi_2{}^l \\ \vdots \\ \vdots \\ \Phi_M{}^l \end{bmatrix}$$

Let $$BW = \begin{bmatrix} B'(1) & C(1) & 0 & 0 & 0 \\ A(2) & B(2) & C(2) & 0 & 0 \\ 0 & A(3) & B(3) & \ddots & 0 \\ 0 & 0 & \ddots & \ddots & C(M-1) \\ 0 & 0 & 0 & A(M) & B'(M) \end{bmatrix}$$

$$\text{and } FW = \begin{bmatrix} E'(1) & F(1) & 0 & 0 & 0 \\ D(2) & E(2) & F(2) & 0 & 0 \\ 0 & D(3) & E(3) & \ddots & 0 \\ 0 & 0 & \ddots & \ddots & F(M-1) \\ 0 & 0 & 0 & D(M) & E'(M) \end{bmatrix}$$

Then field at the next step z+ Δz will be

$$\begin{bmatrix} \Phi_1^{l+1} \\ \Phi_2^{l+1} \\ \vdots \\ \vdots \\ \Phi_M^{l+1} \end{bmatrix} = [BW]^{-1} \times FW \times \begin{bmatrix} \Phi_1^{l} \\ \Phi_2^{l} \\ \vdots \\ \vdots \\ \Phi_M^{l} \end{bmatrix} \tag{2.88}$$

From the equation (2.88) by the knowledge of matrixes BW, FW and field Φ^l we can calculate the field at the next step. This process can be used for certain distance z.

Chapter 3

ACCURACY OF THE SOFTWARE

Accuracy is primary and essential condition for any software to be valid for further use. To prove the accuracy of this software, one comparison is made with Fresnel equation. In this chapter first free space propagation of Gaussian wave is described and its Full width at half maxima (FWHM) is measured. As FWHM can completely describe the shape of the Gaussian profile so FWHM is used to measure the accuracy of the software. Then applying the same excitation as an input to the simulation program and FWHM is measured at same distance. At the end error is calculated between these two FWHM. It is repeated for different spacing (Δz). Among all these error, the minimum one is considered for the further calculation of the different waveguide structures.

Initial conditions considered to make comparison is as follows:-

- Computational window size = 51μm
- Wavelength = 1.00 μm
- No of points in the x-axis = 500.
- Initial excitation = Gaussian Profile
- Beam waist of initial Gaussian profile = 3 μm
- Amplitude of Initial Gaussian Profile = 1 Volt
- Refractive index of the medium=1.00

3.1 Laser Beam Propagation

In general, laser-beam propagation can be approximated by assuming that the laser beam has an ideal Gaussian intensity profile, corresponding to the theoretical TEM_{00}

mode. The TEM_{00} mode output of a laser is a spherical Gaussian beam. The wavefront normals (rays) of a plane wave are parallel to the direction of the wave so that there is no angular spread, but the energy extends spatially over the entire space. The spherical wave, on the other hand, originates from a single point, but its wavefront normals (rays) diverge in all directions. Waves with wavefront normals making small angles with the z axis are called paraxial waves. They must satisfy the paraxial Helmholtz equation. A solution of this equation is a wave called the Gaussian beam. The intensity distribution in any transverse plane is a Gaussian function centered about the beam axis. The width of this function is minimum at the beam waist and grows gradually in both directions. The wavefronts are approximately planar near the beam waist, but they gradually curve and become approximately spherical far from the waist.

The Gaussian Beam

A paraxial wave is a plane wave $\exp(-jkz)$ (with wavenumber $k = 2\pi / \lambda$ and wavelength λ) modulated by a complex envelope $A(r)$ that is a slowly varying function of position. The complex amplitude is [16]

$$U(r) = A(r)\exp(-jkz) \tag{3.1}$$

For the complex amplitude $U(r)$ to satisfy the Helmholtz equation, $V^2U + k^2U = 0$,the complex envelope $A(r)$ must satisfy the paraxial Helmholtz equation [16]

$$\Delta_T^2 A - j2k\frac{\partial A}{\partial z} = 0 \tag{3.2}$$

Where $\Delta_T^2 = \frac{\partial^2}{\partial x^2} + \frac{\partial^2}{\partial y2}$ is the transverse part of the Laplacian operator. One solution to the paraxial Helmholtz equation is paraboloidal wave for which

$$A(r) = \frac{A_1}{z}\exp(-jk\frac{\rho^2}{2z}), \text{ where } \rho^2 = x^2 + y^2 \qquad 3.3)$$

The paraboloidal wave is the paraxial approximation of the spherical wave $U(r) = (A/r)\exp(-jkr)$ when x and y are much smaller than z .Another solution of the paraxial Helmholtz equation provides the Gaussian beam. It is obtained from the paraboloidal wave by use of a simple transformation. Since the complex envelope of the paraboloidal wave equation (3.3) is a solution of the paraxial Helmholtz equation (3.2), a shifted version of it, with $z-\xi$ replacing z where ξ is a constant, and the solution is

$$A(r) = \frac{A_1}{q(z)}\exp\left[-jk\frac{\rho^2}{2q(z)}\right], \qquad q(z) = z - \xi \qquad (3.4)$$

This provides a paraboloidal wave centered about the point $z = \xi$ instead of $z = 0$. When ξ is purely imaginary(ξ = -jz_0 ,where z_0 is real,) equation (3.4) gives rise to the complex envelope of the Gaussian beam as follows

$$A(r) = \frac{A_1}{q(z)}\exp\left[-jk\frac{\rho^2}{2q(z)}\right], q(z) = z + jz_0 \qquad (3.5)$$

The parameter z_0 is known as the Raleigh range.

We can write the complex function $1/q(z) = 1/(z + jz)$ in terms of its real and imaginary parts as

$$\frac{1}{q(z)} = \frac{1}{R(z)} - j\frac{\lambda}{\pi W^2(z)} \qquad (3.6)$$

W(z) and *R(z)* are beam width and wave front radius of curvature, respectively. An expression for the complex amplitude *U(r)* of the Gaussian beam is obtained by Substituting equation. (3.6) into equation.(3.5) and using equation.(3.1) as

$$U(r) = A_0\frac{W_0}{W(z)}\exp\left[-\frac{\rho^2}{W^2(z)}\right]\exp\left[-jkz - jk\frac{\rho^2}{2R(z)} + j\xi(z)\right] \qquad (3.7)$$

The beam parameters can be evaluated by following equations

$$W(z) = W_0\left[1+\left(\frac{z}{z_0}\right)^2\right]^{1/2} \tag{3.8}$$

$$R(z) = z\left[1+\left(\frac{z_0}{z}\right)^2\right] \tag{3.9}$$

$$\xi(z) = \tan^{-1}\left(\frac{z}{z_0}\right) \tag{3.10}$$

$$W_0 = \left(\frac{\lambda z_0}{\pi}\right)^{1/2} \tag{3.11}$$

Now consider a beam wave $U_0(r)$ propagating in the z direction in free space .At the transmitting aperture (z=0), the wave has a Gaussian amplitude distribution with beam size W_0 and a curved phase front with radius of curvature R_0.Then

$$U_0(0,\rho) = \exp\left[-\left(\frac{1}{W_0^2}+j\frac{k}{2R_0}\right)\rho^2\right] \tag{3.12}$$

where $k=\frac{2\pi}{\lambda}$ is wave number, λ is wavelength, ρ is the radial vector from the z axis.

We can also write Equation. (3.12) as [15]

$$U_0(0,\rho) = \exp\left[-\frac{1}{2}k\alpha\rho^2\right] \tag{3.13}$$

where $\alpha = \alpha_1 + j\alpha_2 = \frac{\lambda}{\pi W_0^2} + j\frac{1}{R_0}$

at an arbitrary point (ρ, z) the beam in free space is given by

$$U_0(\rho,z) = \frac{1}{(1+j\alpha z)}\exp\left[jkz-\left(\frac{k\alpha}{2}\right)\frac{\rho^2}{(1+j\alpha z)}\right] \tag{3.14}$$

this is valid within a distance z [15] such that

$$z << \frac{\pi^3 W_0^4}{\lambda^3} \tag{3.15}$$

which covers almost all the laser propagation distances used in practice. The effect on the beam parameters as beam advances is described below.

Intensity

The optical intensity $I(r) = |U(r)|^2$ is a function of the axial and radial distances z and $\rho = (x^2 + y^2)^{1/2}$,

$$I(\rho, z) = I_0 \left[\frac{W_0}{W(z)}\right]^2 \exp\left[-\frac{2\rho^2}{W^2(z)}\right] \tag{3.16}$$

Where $I_0 = |U_0|^2$. At each value of z the intensity is a Gaussian function of the radial distance ρ. The Gaussian function has its peak at ρ = 0 (on axis) and drops monotonically with increasing ρ. The width $W(z)$ of the Gaussian distribution increases with the axial distance z as illustrated in Fig.3.1

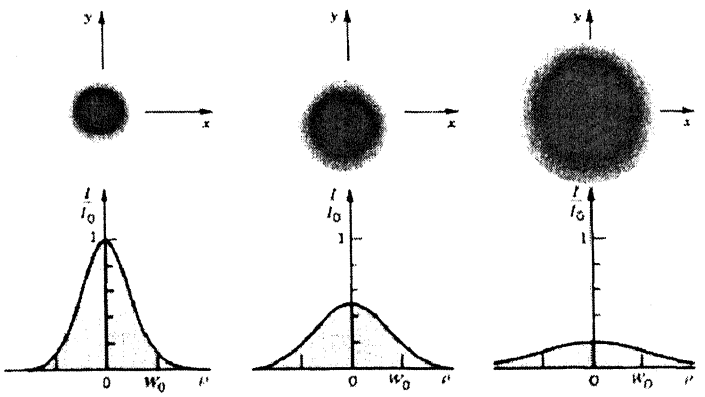


Figure 3.1 The normalized beam intensityI/I$_0$ as a function of the radial distance ρ at different axial distances: (a) z = 0 (b) z = z$_0$ (c) z = 2z$_0$ [16]

On the beam axis (ρ = 0) the intensity can be given by[15]

$$I(0, z) = I_0 \left[\frac{W_0}{W(z)}\right]^2 = \frac{I_0}{1 + (z/z_0)^2} \tag{3.17}$$

It has maximum value I_0 at $z = 0$ and drops gradually with increasing z, reaching half of its peak value at $z = +z_0$ (figure 3.2). When $|z| >> z_0$, $I(0,z) \approx I_0 z_0^2/z$ so that the intensity decreases with the distance in accordance with an inverse-square law. The overall peak intensity $I(0, 0) = I_O$ occurs at the beam center ($z = 0$, $\rho = 0$).

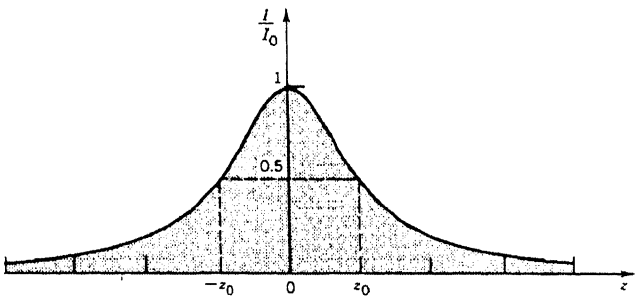


Figure 3.2 The normalized beam intensity I/I_0 at points on the beam axis ($\rho = 0$) as a function of z [16].

Power

The total optical power carried by the beam is the integral of the optical intensity over a transverse plane (at a distance z),

$$P = \int I(\rho,z)2\pi\rho d\rho, \quad P = \frac{1}{2} I_0(\pi W_0^2) \tag{3.18}$$

Since beams are often described by their power P, it is useful to express I, in terms of P as[15]

$$I(\rho,z) = \frac{2P}{\pi W^2(z)} \exp\left[-\frac{2\rho^2}{W^2(z)}\right] \tag{3.19}$$

The ratio of the power carried within a circle of radius ρ_0 in the transverse plane at position z to the total power is

$$\frac{1}{p}\int_0^{\rho_0} I(\rho,z)2\pi\rho d\rho = 1 - \exp\left[-\frac{2\rho_0^2}{W^2(z)}\right] \tag{3.20}$$

Beam Radius

Within any transverse plane, the beam intensity assumes its peak value on the beam axis, and drops by the factor $1/e^2 = 0.135$ at the radial distance $\rho = W(z)$. Since 86% of the power is carried within a circle of radius $W(z)$, $W(z)$ is regarded as the beam radius (also called the beam width). The rms width of the intensity distribution is $\sigma = \frac{1}{2}W(z)$. The dependence of the beam radius on z is governed by

$$W(z) = W_0\left[1+\left(\frac{z}{z_0}\right)^2\right]^{1/2} \tag{3.21}$$

It assumes its minimum value W_0 in the plane $z = 0$, called the beam waist. Thus W_0 is the waist radius. The waist diameter $2W_0$ is called the spot size. The beam radius increases gradually with z, reaching $\sqrt{2}W_0$, at $z = z_0$, and continues increasing monotonically with z as shown in Figure 3.3. For $z >> z_0$,

$$W(z) \approx \frac{W_0}{z_0}z = \theta_0 z \tag{3.22}$$

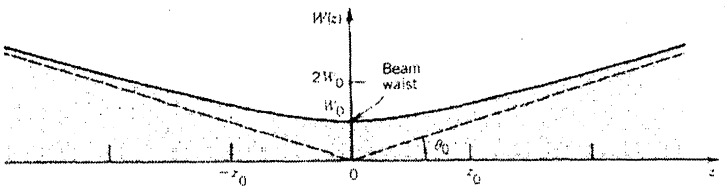


Figure 3.3 Beam radius as a function of propagation distance.[16]

where $\theta_0 = W_0/z_0$. Using equation.(3.22) and equation.(3.11) we can also write

$$\theta_0 = \frac{\lambda}{\pi W_0} \tag{3.23}$$

Beam Divergence

when $z >> z_0$, the beam radius increases approximately linearly with z, defining a cone with half-angle θ_0.About 86% of the beam power is confined within this cone. The angular divergence of the beam is therefore defined by the angle

$$\theta_0 = \frac{2}{\pi}\frac{\lambda}{2W_0} \tag{3.24}$$

The beam divergence is directly proportional to the ratio between the wavelength λ and the beam-waist diameter $2W_0$.

Depth of Focus

The axial distance within which the beam radius lies within a factor $\sqrt{2}$ of its minimum value is known as the depth of focus. The depth of focus is twice the Rayleigh range. Since the beam has its minimum width at z = 0, as shown in figure 3.3, it achieves its best focus at the plane z = 0. In either direction, the beam gradually grows "out of focus."

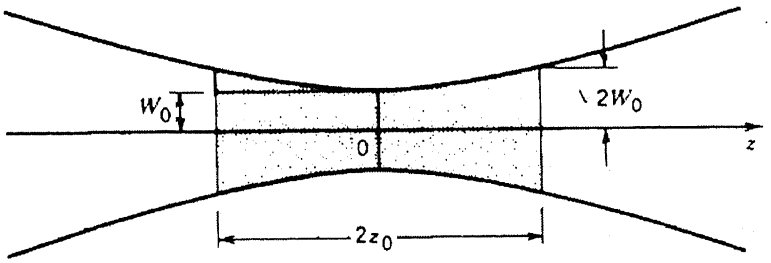


Figure 3.4 The depth of focus of a Gaussian beam.[16]

Hence depth of focus is given by

$$2z_0 = \frac{2\pi W_0^2}{\lambda} \tag{3.25}$$

Phase

The dependence of phase of the Gaussian beam on the distance is given by

$$\varphi(\rho, z) = kz - \xi(z) + \frac{k\rho^2}{2R(z)} \tag{3.26}$$

On the beam axis ($\rho = 0$) the phase is

$$\varphi(0, z) = kz - \xi(z) \tag{3.27}$$

Where kz phase of plan wave and $\xi(z)$ is phase retardation.

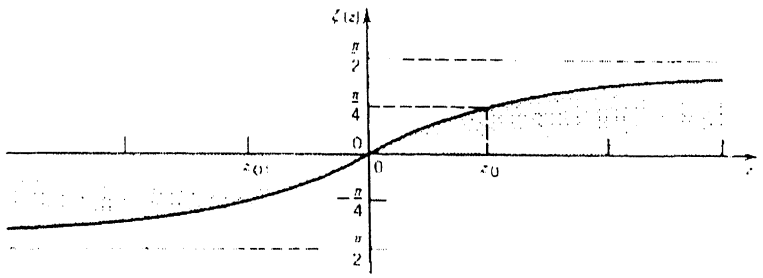


Figure 3.5 Phase retardation of the Gaussian beam relative to a uniform planewave at points on the beam axis.[16]

3.1.1 FWHM calculation by FRESNEL equation for the Gaussian Propagation

To validate the FDBPM code we have compared the result of FDBPM with known result. so we have analyzed the propagation of Gaussian beam in free space. Using the Gaussian wave as an initial excitation with beam waist 3um we propagated upto 400um. At 400um we have calculated the FWHM of the profile which is 5.02e-05um.

3.2 FWHM calculation by FDBPM

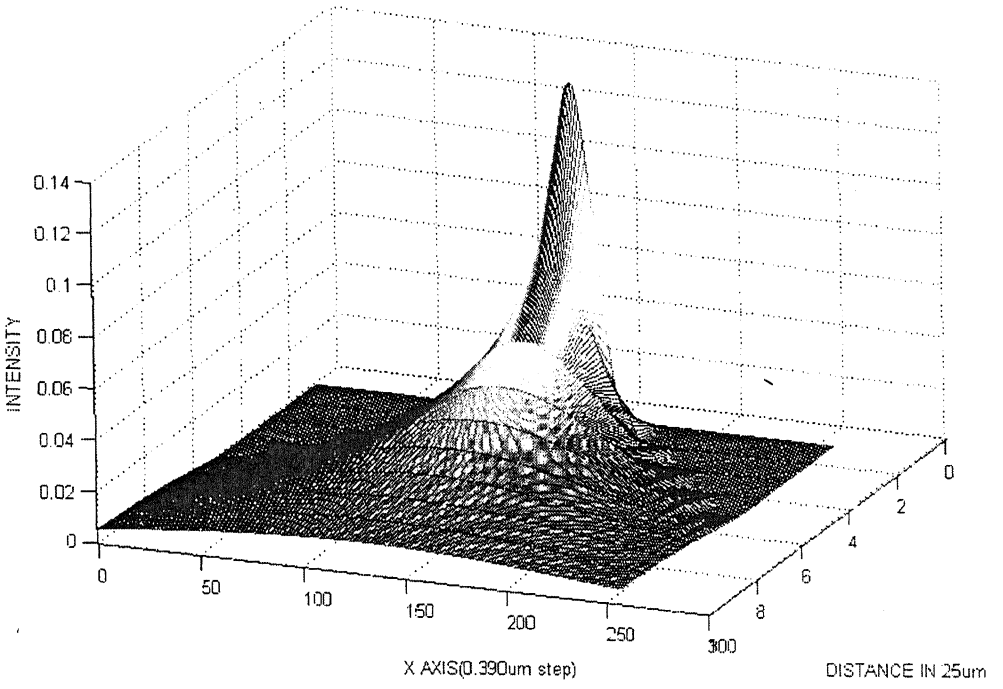


Figure 3.6 Free space Propagation of Gaussian Wave

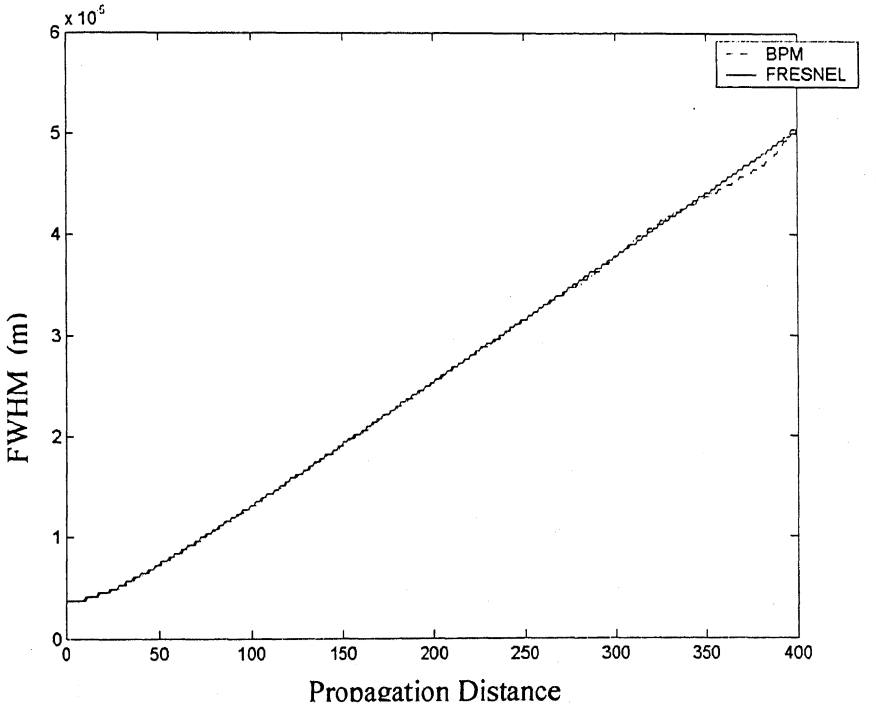


Figure3.7 FWHM calculated by FDBPM and FRESNEL calculation

3.3 Error calculation in FWHM measured by FD BPM

S.NO	DELTAZ (meter)	FWHM(FDBPM) (meter)	FWHM(FRESNEL) (meter)	ERROR (percentage)
1	1.000e-005	4.158e-004	4.158e-005	1.717e+001
2	5.000e-006	5.020e-004	5.020e-005	0.000e+000
3	2.000e-006	5.020e-004	5.020e-005	0.000e+000
4	1.000e-006	5.020e-004	5.020e-005	0.000e+000
5	5.000e-007	5.020e-004	5.020e-005	0.000e+000

Table3.1 Error in FWHM measured by FDBPM

In the figure 3.8 the variation of the error in FWHM with the distance can be seen.

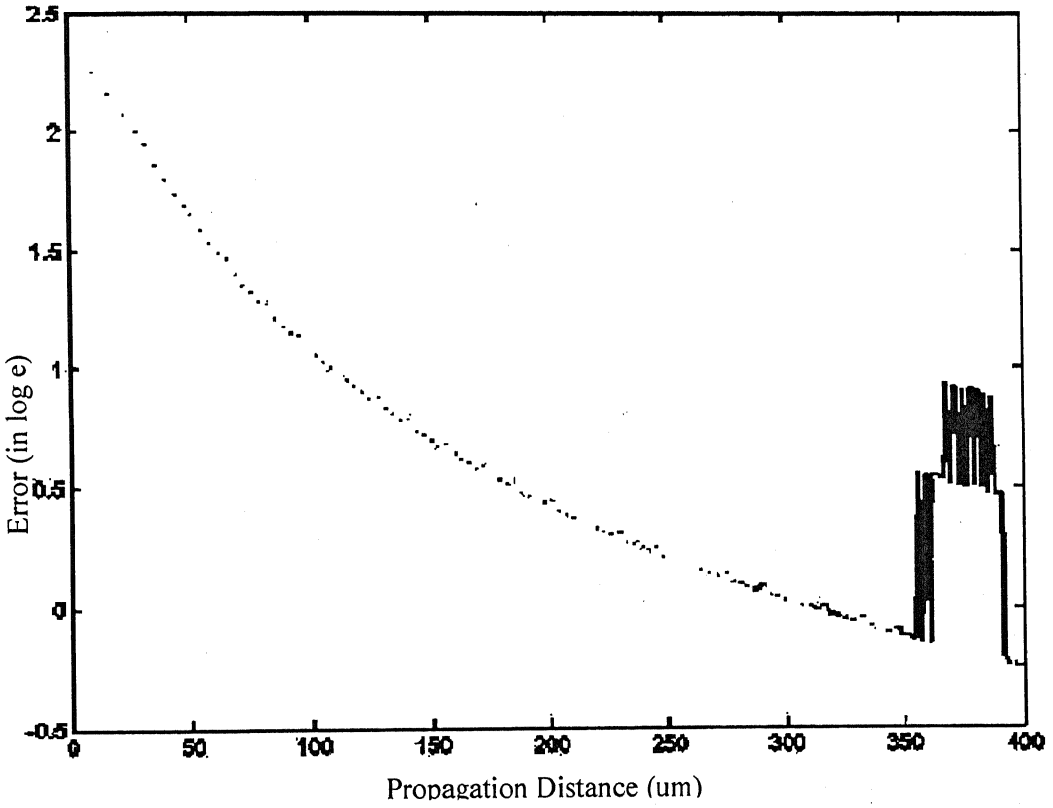


Figure 3.8 Error in FWHM by Fresnel equation and FWHM by FDBPM

Figure 3.7 shows that FWHM measured by FDBPM is approaching the FWHM of the fresnel equation. Now form table 3.1 it was observed that with $\Delta z = 1\mu m$ the error was considerable less. So for further calculation I have taken $\Delta z = \lambda$. We have used the matlab to calculate the error which is accurately calculating floating point value upto 32 total bits and 8 exponential bits.

3.4 Mode Calculation Theory

Since the Propagation constant in the z direction is given by $\exp(-i\beta z)$ so equation(2.14) chapter2 will become

$$\frac{\partial^2 E_y}{\partial x^2} = [\beta^2 - \omega^2 \mu\varepsilon] E_y \tag{3.28}$$

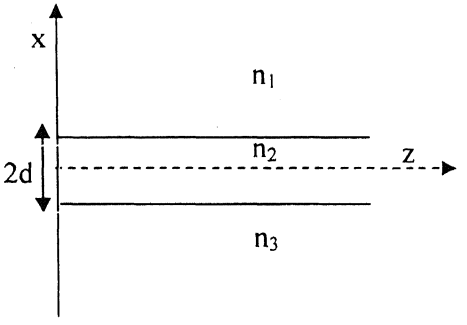


Figure 3.9 Slab Waveguide Structure

Solution of the equation (3.28) can be expressed as

$$E_y(x) = C_1 \cos k_{1x} x \qquad \text{for } -d \le x \le d \tag{3.29}$$

$$E_y(x) = C_1 \sin(k_{1x} x) \qquad \text{for } -d \le x \le d \tag{3.30}$$

$$k_{1x}^2 = \omega^2 \mu\varepsilon_1 - \beta^2 = k_1^2 - \beta^2 \tag{3.31}$$

$$E_y(x) = D_1 \exp(-\alpha_2 x) \qquad \text{for} \qquad x > d \tag{3.32}$$

$$\alpha_2^2 = \beta^2 - \omega^2 \mu\varepsilon_2 = \beta^2 - k_2^2 \tag{3.33}$$

Where C_1 and D_1 are constants.

At the boundary both field are same so the field equation (3.32) will become

$$E_y(x) = C_1 \cos(k_{1x}x)\exp[-\alpha_2(x-d)] \tag{3.34}$$

At the boundary of two medium value of magnetic field $H_{1z} = H_{2z}$. The value of H_z can be calculated from equation(2.12)

$$-\frac{ik_{1x}}{\omega\mu} C_1 \sin(k_{1x}d) = -\frac{i\alpha_2}{\omega\mu} C_1 \cos(k_{1x}d) \tag{3.35}$$

$$\tan(k_{1x}d) = \frac{\alpha_2}{k_{1x}} \tag{3.36}$$

Using $\sin(k_{1x}d)$ as a solution again applying boundary condition $H_{1z} = H_{2z}$ we get

$$\tan(k_{1x}d) = -\frac{k_{1x}}{\alpha_2} \tag{3.37}$$

Using equation(3.31) , equation(3.33) we can write

$$\alpha_2{}^2 = k_0{}^2[n_1{}^2 - n_2{}^2] - k_{1x}{}^2 \tag{3.38}$$

Normalized frequency variable V is given by

$$V^2 = [n_1{}^2 - n_2{}^2]k_0{}^2 d^2 \tag{3.39}$$

Using equation (3.38) and equation (3.39) becomes

$$V^2 = \alpha_2{}^2 d^2 + k_{1x}{}^2 d^2 \tag{3.40}$$

We can get the solution of equation(3.36) and equation(3.37) by using the equation(3.40) . The number of solution of equation(3.36) and equation(3.37) have same number of modes will propagating in the slab waveguide.

3.5 Verification of result for Waveguide

Assuming the following data for the slab waveguide mode verification.

Width of core =6um

Core Refractive Index=1.500

Cladding Refractive Index=1.495

Wavelength = 1um.

Using Mathematical analysis with equation (3.36), equation (3.37) and equation (3.40) we get only one solution. Which shows that only one mode is propagating inside the slab waveguide as shown in figure 3.10.

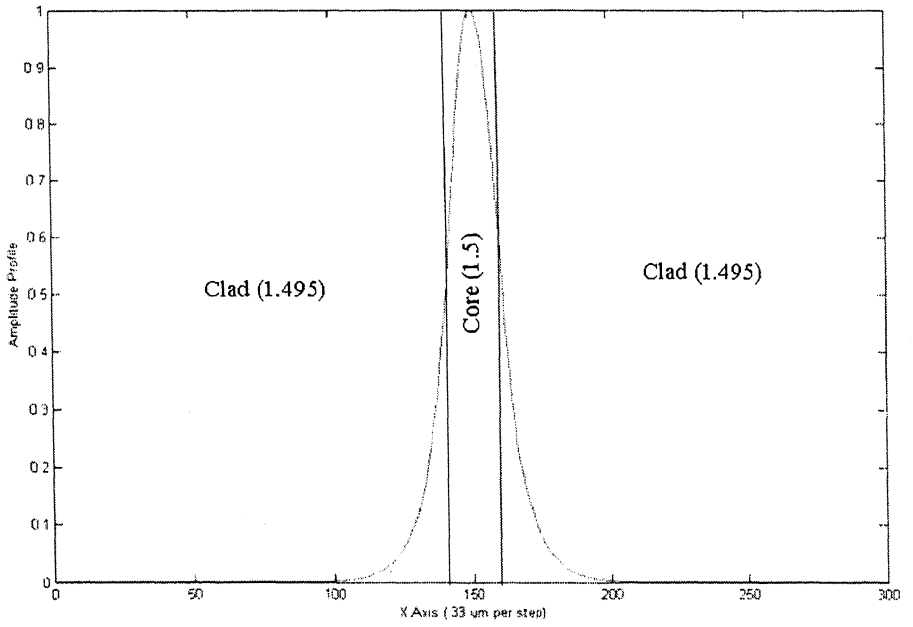


Figure 3.10 Amplitude Profile of Slab Waveguide structure by calculation

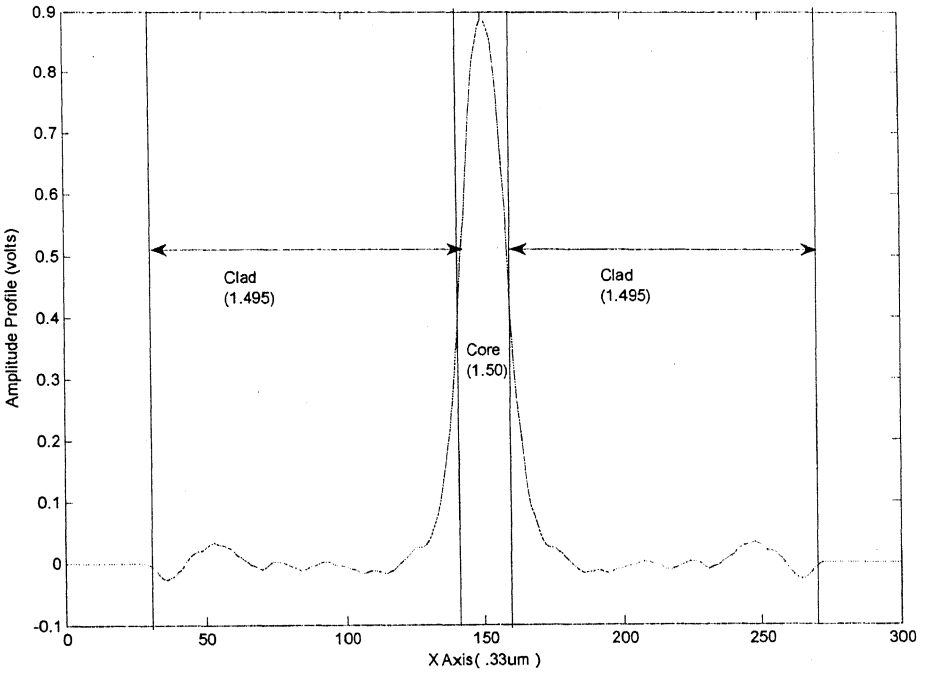


Figure 3.11 Amplitude Profile of Slab Waveguide structure by FDBPM

Using the numerical method also we get the field profile as shown in the figure 3.1 1 Which shows that we are getting the single mode propagation inside the slab waveguide.

From the above analysis it can be concluded that FDBPM is suitable for waveguide structures. Which will be used for further analysis of the perturbation in waveguide.

Chapter 4

RESULTS AND DISCUSSION

During the first stage of the work, a FD BPM code considering the transversal electric field component is made and validated by free space Gaussian beam propagation. In the second stage, FDBPM is used for analysis of slab waveguide structure. Single mode and multimode analyses of slab waveguide structure are discussed in this section. Then, by FDBPM code, perturbed slab waveguide is also analyzed. The effect of different refractive indexes of the surrounding medium is also tested.

4.1 Free Space Propagation

Using FDBPM code we can see the intensity profile after launching the Gaussian excitation as an input for free space propagation.

4.1.1 FDBPM without Boundary Condition

As we analysis the physical structure numerically we can not analyze the structure for infinite width. We have to analyze the structure within the certain boundary. As we go out from the computational window their sudden change in the window so that due this change some reflection starts coming back into the computational window. Figure (4.1) shows the intensity profile using FDBPM without applying the boundary condition

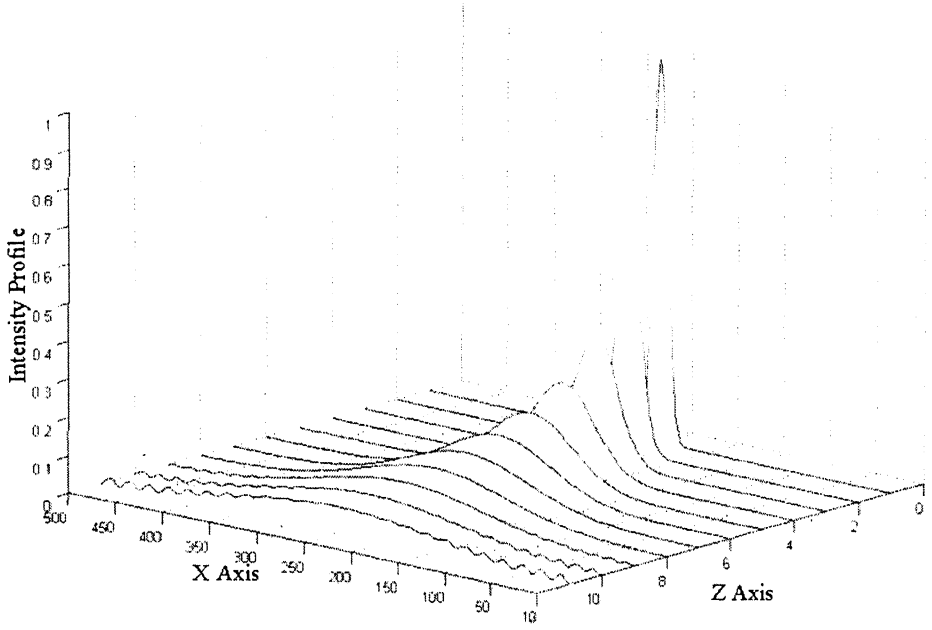


Figure (4.1) Intensity profile without boundary condition

4.1.2 FDBPM with Boundary Condition

To remove the reflections coming from the boundary we apply the boundary condition. The following figure (4.2) shows the intensity profile using FDBPM with Transparent boundary condition

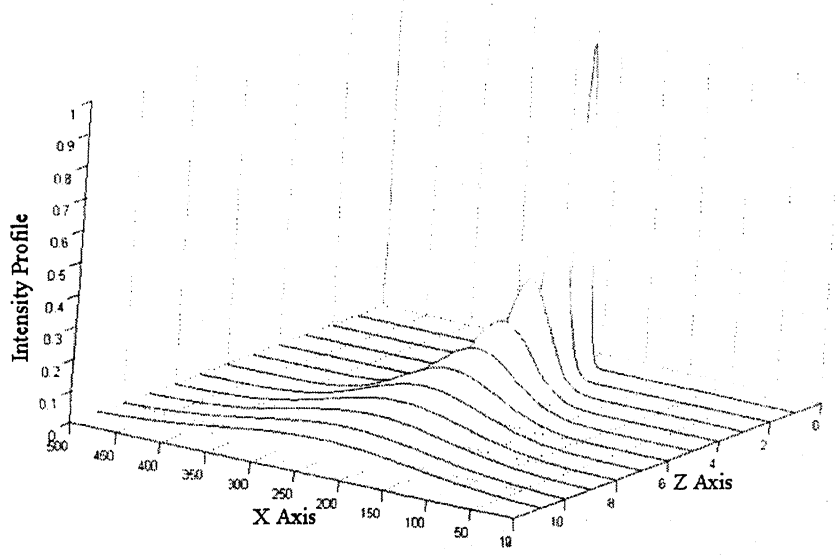


Figure (4.2) Intensity profile with boundary condition

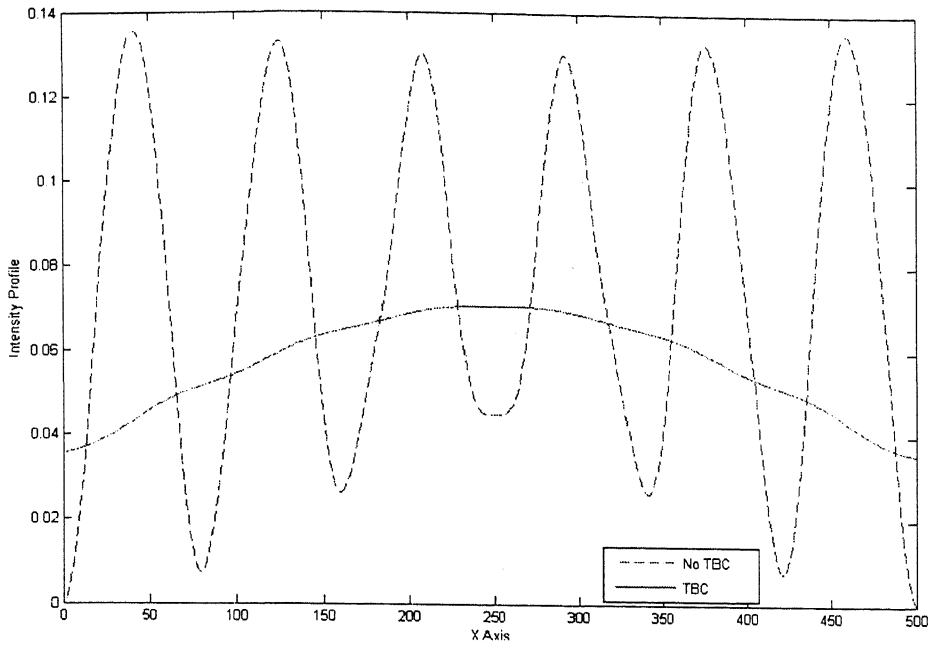


Figure (4.3) Intensity profile at 400um

From figure(4.1) and figure(4.2) we can see the significance of the boundary condition applied to the computational window. Figure (4.3) illustrates the interference pattern formed by the reflections in the presence of the computational boundaries and effect of TBC at 400um.

4.2 Singlemode and Multimode Waveguide Structure Analyses

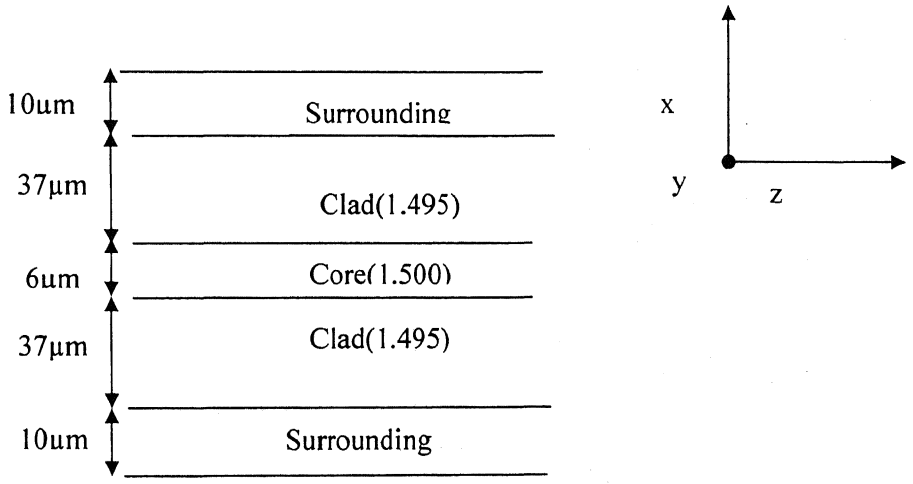


Figure (4.4) Slab Waveguide Structure

From section (3.5) chapter 3 we can see that existing code can be applied for slab waveguide structure. Using slab waveguide structure (figure (4.4)) the intensity profile of the single mode propagation was calculated, as illustrated in figure (4.5) .

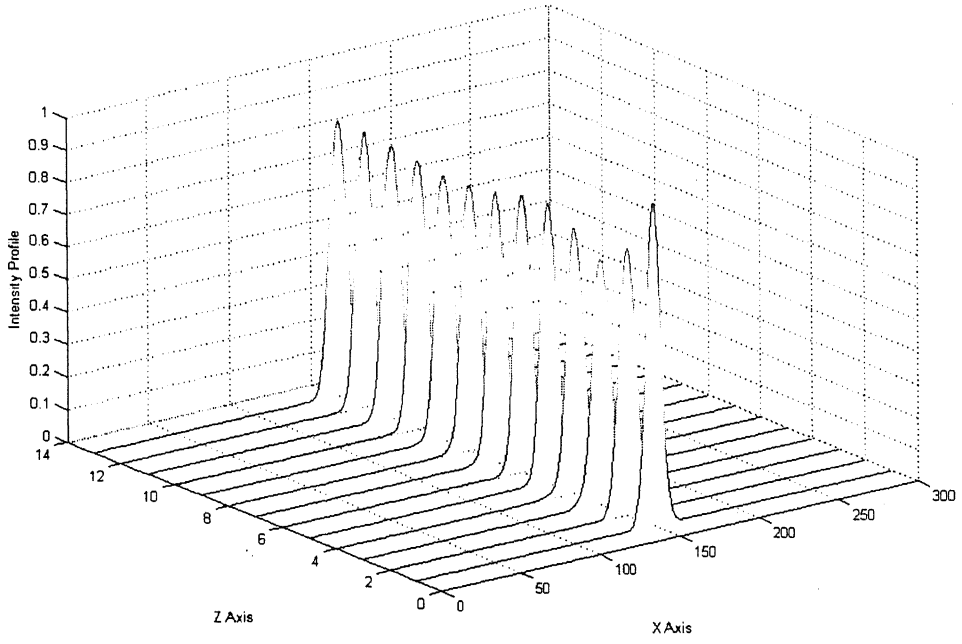


Figure 4.5 Single Mode Intensity profile

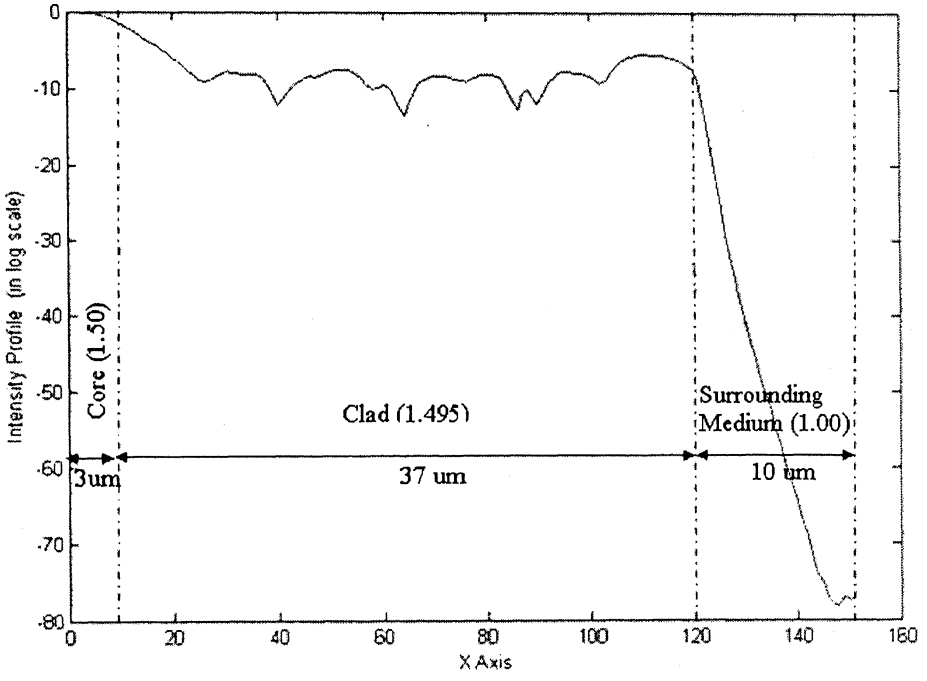


Figure 4.6 Half of the Intensity Profile at Output

The effect of change in core width on the intensity profile of the structure was also analyzed. We varied the core width from $6\,\mu m$ to $12\,\mu m$. We can see from the intensity profiles shown in figure (4.5) and figure (4.7) that single mode profile is converted into the multimode profile which is the effect of increase in the core width. It can inferred from this result that increase in the core width results the increase in number of mode. It was also observed that the amplitude of the intensity profile repeats in the periodic interval (figure (4.7)).

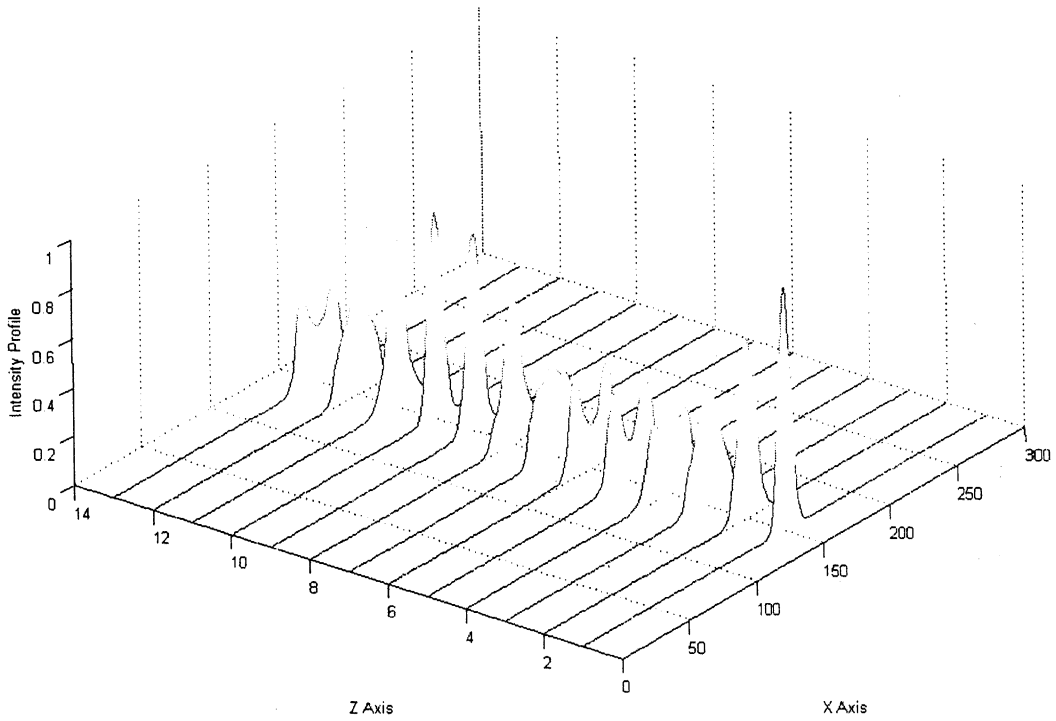


Figure (4.7) Top View of the intensity profile using multimode structure

Figure 4.8 illustrates the intensity profile for single mode and multimode structures while keeping surrounding medium as air at distance of 1cm.

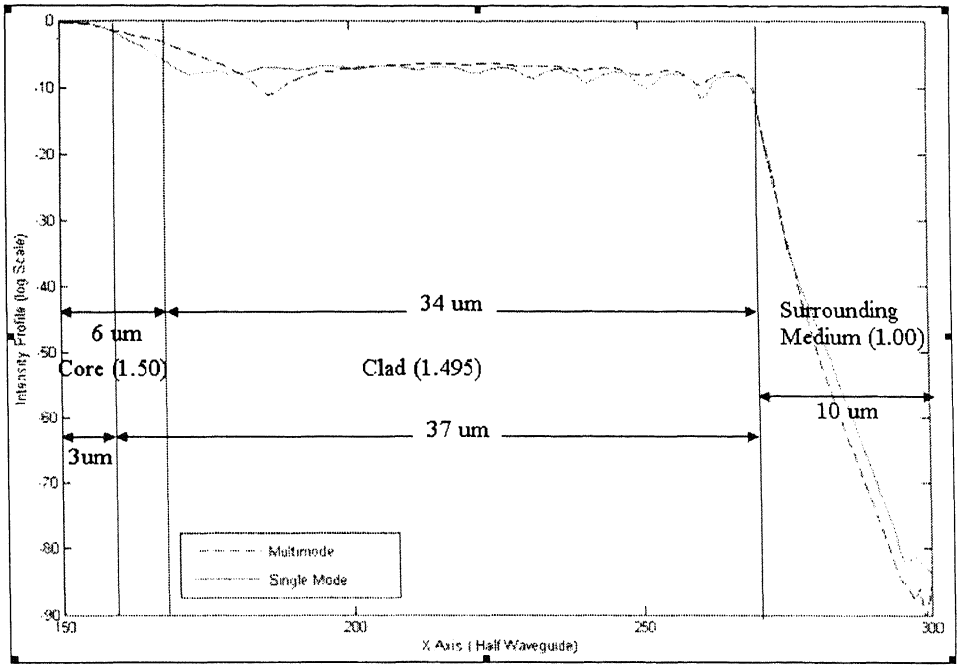


Figure (4.8) Intensity Profile of single mode and multimode structure

4.3 Power Calculation

In this thesis research we have tried to implement the refractive index sensors. This sensors works sense different refractive index accordingly change in output power. As we move along Z direction we get the intensity profile which is stabilized after 200um of propagation from the start of excitation.

We can get the power P form the intensity profile I which is defined between interval x_1 and x_2 is defines as $P = \int_{X_1}^{X_2} Idx$. Here we get the power form the intensity profile by numerical integration method. Now a days there are two famous techniques used for numerical integration.

4.3.1 Trapezoidal Method

The Trapezoidal Method is a numerical method for estimating the value of an integral $\int_a^b f(x)dx$ or estimating the area under a curve generated by a function f(x). A linear function, which is the simplest polynomial approximation, is the basis of the Trapezoidal Method. As the name suggests, the Trapezoidal Method is based on taking the area of trapezoids after a given function f(x) has been approximated by a linear function

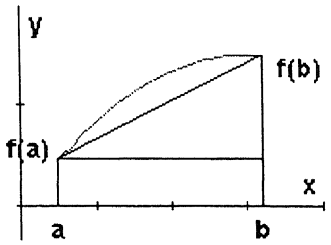


Figure 4.9 Trapezoid area calculation for two points

The area of the trapezoid is just the area of the rectangle plus the area of the triangle. That means our approximation is

$$\int_a^b f(x)dx = (b-a)f(a) + \frac{1}{2}(b-a)[f(b)-f(a)] \tag{4.1}$$

$$= (b-a)[f(a) + \frac{1}{2}f(b) - \frac{1}{2}f(a)] \tag{4.2}$$

$$= \frac{1}{2}(b-a)[f(a)+f(b)] \tag{4.3}$$

we cannot expect this to be a good approximation. However, we can break the region $[a,b]$ into many smaller pieces and apply the approximation on each piece. On the smaller pieces, the graph looks more and more like a straight line so the

approximation should improve. Let's choose some positive integer **n** and break the interval $[a,b]$ into **n** equal pieces. The width of each piece is $h=\frac{b-a}{n}$.

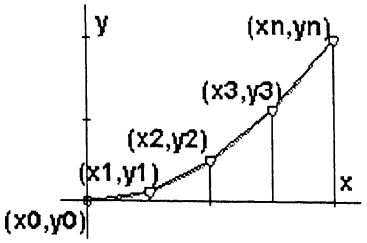


Figure 4.10 Trapezoid area calculation for more points

We will label the points defined by the sub-intervals by x_i and call $y_i = \int f(x_i)dx$. If we the approximate the area under the graph by the area of the trapezoids, we have

$$\int_a^b f(x)dx \approx T_n = \frac{h}{2}(y_0+y_1)+\frac{h}{2}(y_1+y_2)+....\frac{h}{2}(y_{n-1}+y_n) \tag{4.4}$$

$$=\frac{h}{2}[y_0+y_1+y_1+y_2+y_2+y_3+.....+y_n] \tag{4.5}$$

$$=\frac{h}{2}[y_0+2y_1+2y_2+2y_3+.....+2y_{n-1}+y_n] \tag{4.6}$$

4.3.2 Simpson's Rule

Simpson's rule is a approximating the integral of a function f using quadratic polynomials (i.e., parabolic arcs instead of the straight line segments used in the trapezoidal rule). Simpson's rule can be derived by integrating a third-order Lagrange interpolating polynomial fit to the function at three equally spaced points. In

particular, let the function f be tabulated at points x_0, x_1, and x_2 equally spaced by distance h, and denote $f_n = f(x_n)$. Then Simpson's rule states that

$$\int_{x_0}^{x_1} f(x)dx = \int_{x_0}^{x_0+2h} f(x)dx \tag{4.7}$$

$$\approx \frac{1}{3}h(f_0 + 4f_1 + f_2) \tag{4.8}$$

Since it uses quadratic polynomials to approximate functions, Simpson's rule actually gives exact results when approximating integrals of polynomials up to cubic degree.

In exact form,

$$\int_{x_0}^{x_2} f(x)dx = \frac{1}{3}h(f_0 + 4f_1 + f_2) + \frac{1}{6}\int_{x_1}^{x_2}(x_0 - t)^2(x_1 - t)f^{(3)}(t)dt$$

$$+\frac{1}{6}\int_{x_1}^{x_2}(x_2 - t)^2(x_1 - t)f^{(3)}(t)dt \tag{4.9}$$

$$= \frac{1}{3}h(f_0 + 4f_1 + f_2) + Rn \tag{4.10}$$

where the remainder term can be written as

$$Rn = \frac{1}{90}h^5 f^{(4)}(x^*) \tag{4.11}$$

with x^* being some value of x in the interval $[x_1, x_2]$.

An extended version of the rule can be written for $f(x)$ tabulated at x_0, x_1, ...,x_{2n} as

$$\int_{x_0}^{x_{2n}} f(x)dx = \frac{1}{3}h[f_0 + 4(f_1 + f_3 + ... + f_{2n-1})$$

$$+2(f_2 + f_4 + ... + f_{2n-2}) + f_{2n}] - Rn \tag{4.12}$$

where the remainder term is

$$Rn = \frac{1}{90}h^5 f^{(4)}(x^*) \tag{4.13}$$

with x^* being some value of x in the interval $[x_1, x_{2n}]$.

4.4 Refractive Index Sensing with Evanescent Field

Optical fiber is partially uncladded and is surrounded by a medium whose refractive index is to be measured. If optical fiber is partially uncladded but removal of cladding is not 100%, some cladding is remains in this case one part of this evanescent wave is transform into a propagating wave. By putting a third medium n_{ext} close to the interface, the evanescent wave is frustrated and a wave propagates into the third medium. This process is called frustrated total reflection [17]. It is given in figure 4.11. In Figure 4.11 d is the thickness of the cladding.

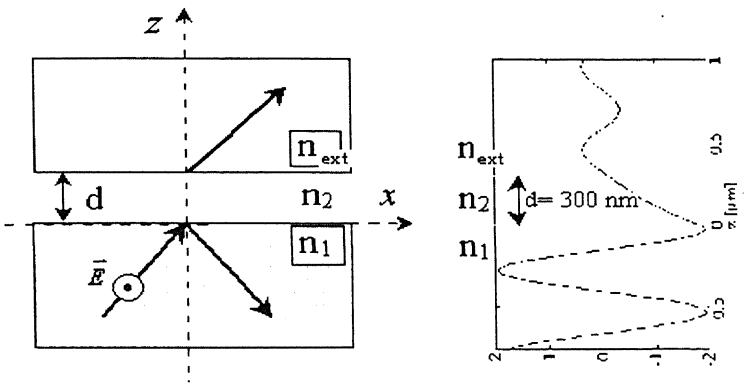


Figure 4.11 Total electric field of the frustrated total reflection process in TE-mode. On the right, the profile in the z-direction is plotted. [17]

4.4.1 Mathematical Analysis of Evanescent Wave Sensor

Evanescent wave sensor works [18,19]. If a portion of the cladding is stripped away and a medium of different refractive index n_{ext} is placed in contact with the fiber core, and we find that for total internal reflection, the angle at which the ray entering at boundary between core and measured refractive index, must be greater than new critical angle:

$$\sin\theta_c = n_{ext} / n_1 \tag{4.14}$$

Different guiding characteristics will apply and the new NA will be given by:

$$\cos\theta_2 = n_{ext} / n_1 \tag{4.15}$$

For the case where core refractive index greater than measured refractive index, if the refractive index of the medium surrounding the exposed fiber core increases so that it approaches the refractive index of the core then the value of new critical angle increases and therefore new NA will decrease. This results in some of the light being lost from the fiber into the surroundings.

When liquid is absorbing; the transmitted light through absorbing medium is given by;

$$I_t = I_0 \exp(-r\alpha L) \tag{4.16}$$

Where L is the length of absorption region and α is the absorption coefficient of the absorbing medium. The fraction of evanescent power, which can be, interacts with the absorbing medium is the quantity closely related to the fraction r, of the total guided power that resides in the cladded region, i.e.

$$r = P_{clad} / P_{total} \tag{4.17}$$

Substantial values (>50%) for r in single mode fibers and for multimode fiber the average fractional power in the cladding is very low (~1%).

4.4.2 Sensitivity of the Sensor

The sensitivity s of a function f(x) to parameter changes can be represented as follows [20,21]:

$$s_{a_i}^{f} = \frac{\Delta f(x)/f(x)}{\Delta a_i / a_i} \tag{4.18}$$

Where a_i , the parameter of interest are core diameter and cladding refractive index.

The sensitivity s of V to changes in n_2 is given by

$$s_{n_2}^{V} = \frac{2n_2}{V}\frac{\partial V}{\partial n_2} = -\frac{2n_2}{V}\frac{\pi a}{\lambda_0}\frac{n_2}{\sqrt{n_1^2 - n_2^2}} \tag{4.19}$$

From depth of penetration, the sensitivity s of d_p as a result of change in n_2 is given by

$$s_{n_2}^{d_p} = \frac{n_2^2 / n_1^2}{(Sin^2\theta - (n_2^2 / n_1^2))} \tag{4.20}$$

The negative sign in equation (4.19) indicates that an increase in the refractive index, n_2, results in a decrease in the number of modes to be propagated into a fiber. The positive sign in (4.20) indicates that the penetration depth increases with cladding refractive index, a reduction in the electric field within the core.

4.4.3 Factors affecting Sensitivity

The various factors affecting the intensity of light lost are wavelength of the light, temperature, length of the fiber (cladded and un-cladded), shape of the fiber (micro bending) in the sensing uncladed region, effect of cladding thickness etc. In this experiment wavelength of light if fixed .The effect of temperature must be minimized to increase accuracy.

4.5 Analysis of Perturbation in Slab Waveguide

In this section first, the different percentage of cross sectional cut in some portion of the cladding is analyzed. Then its effect on Intensity profile and power at the output is observed. Effect of different refractive index is also analyzed at the output. Figure (4.12) and figure (4.13) shows the perturbation in the slab structure. The structure (figure(4.5)) is used as the reference for the power measurement and Intensity Profile calculation (figure(4.5)) at the output end.

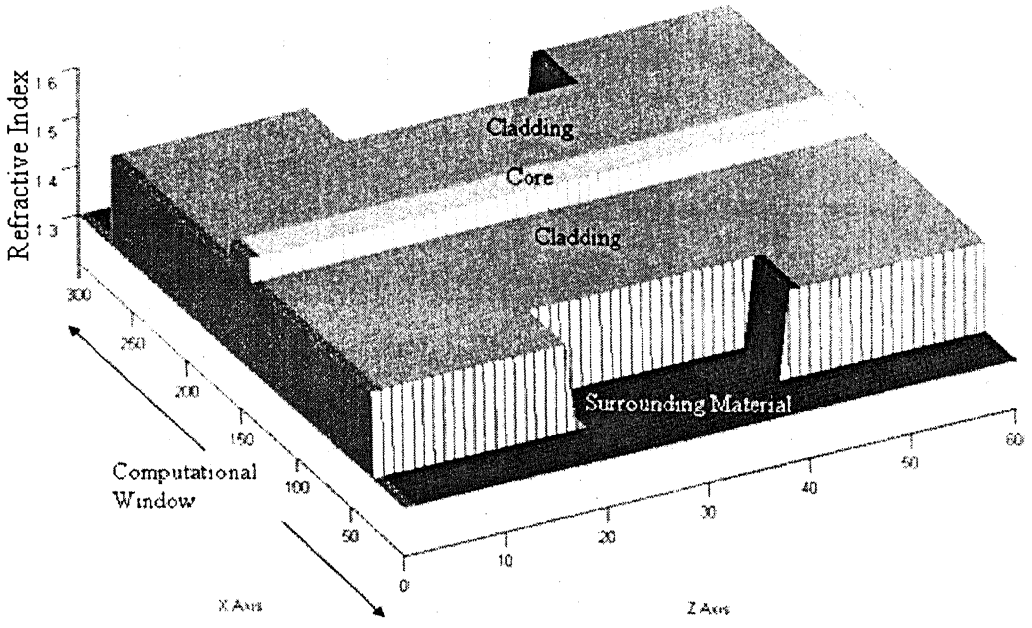


Figure 4.12 Slab waveguide Structure with Cross Sectional Cut(3d view)

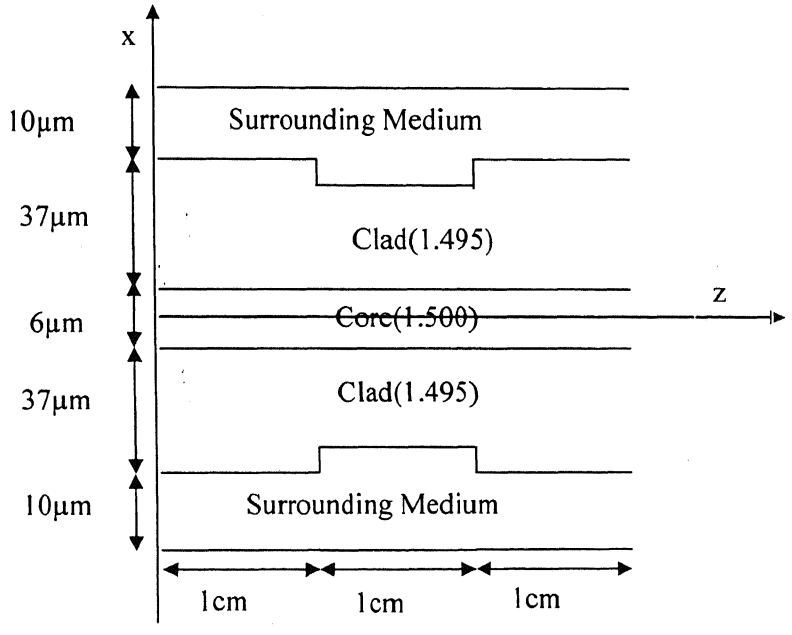


Figure 4.13 Slab Waveguide Structure with Cross Sectional Cut (top view)

पुरुषोत्तम काशीनाथ केलकर पुस्तकालय
भारतीय प्रौद्योगिकी संस्थान कानपुर
प्राप्ति क्र० A 152057

4.5.1 Effect of Cladding Removal

Figure (4.14) illustrates the intensity profile during the propagation. The small increment in the cross sectional percentage cut is causing small decrement in the total output power of core and cladding (at the end). It is shown in the table (4.1) and figure (4.15). This decrement in the output power is due to leakage of more power coupled to the surrounding medium.

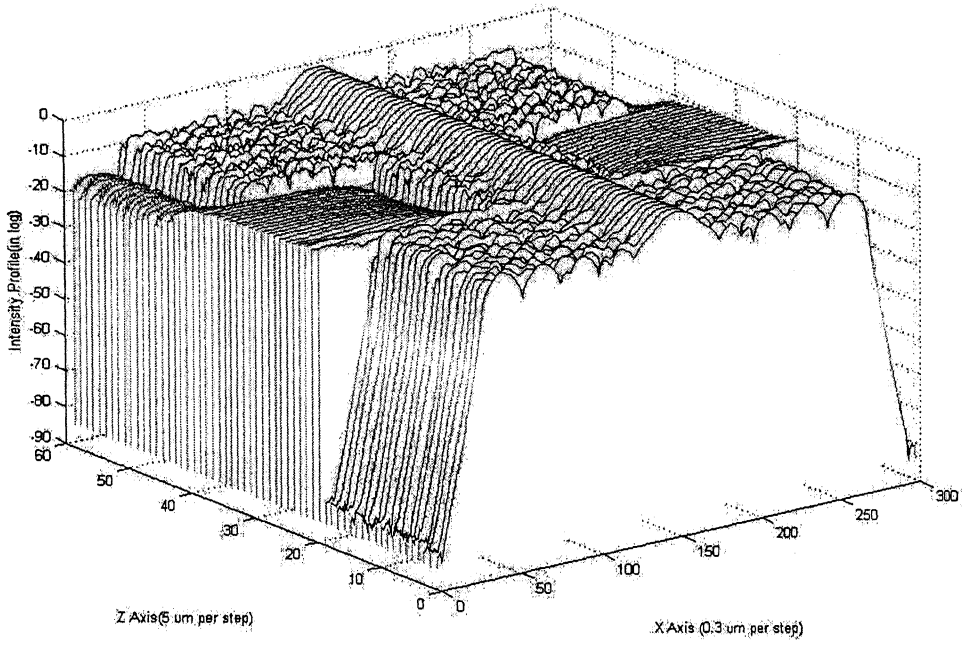


Figure 4.14 Intensity Profile for 70 Percentage of cut in cladding

S.NO	DISTANCE (meter)	CLADDING REMOVAL (In Percentage)	POWER (watt)
1	3.000e-002	00	3.7599e-006
2	3.000e-002	70	3.7426e-006
3	3.000e-002	80	3.7329e-006
4	3.000e-002	90	3.726e-006
5	3.000e-002	100	3.4967e-006
6	3.000e-002	100 percent cladding and 5 percent core	2.7415e-006

Table 4.1 Change in Output Power for Different percentage of cladding

Removal(**Surrounding medium Refractive Index=1.00**)

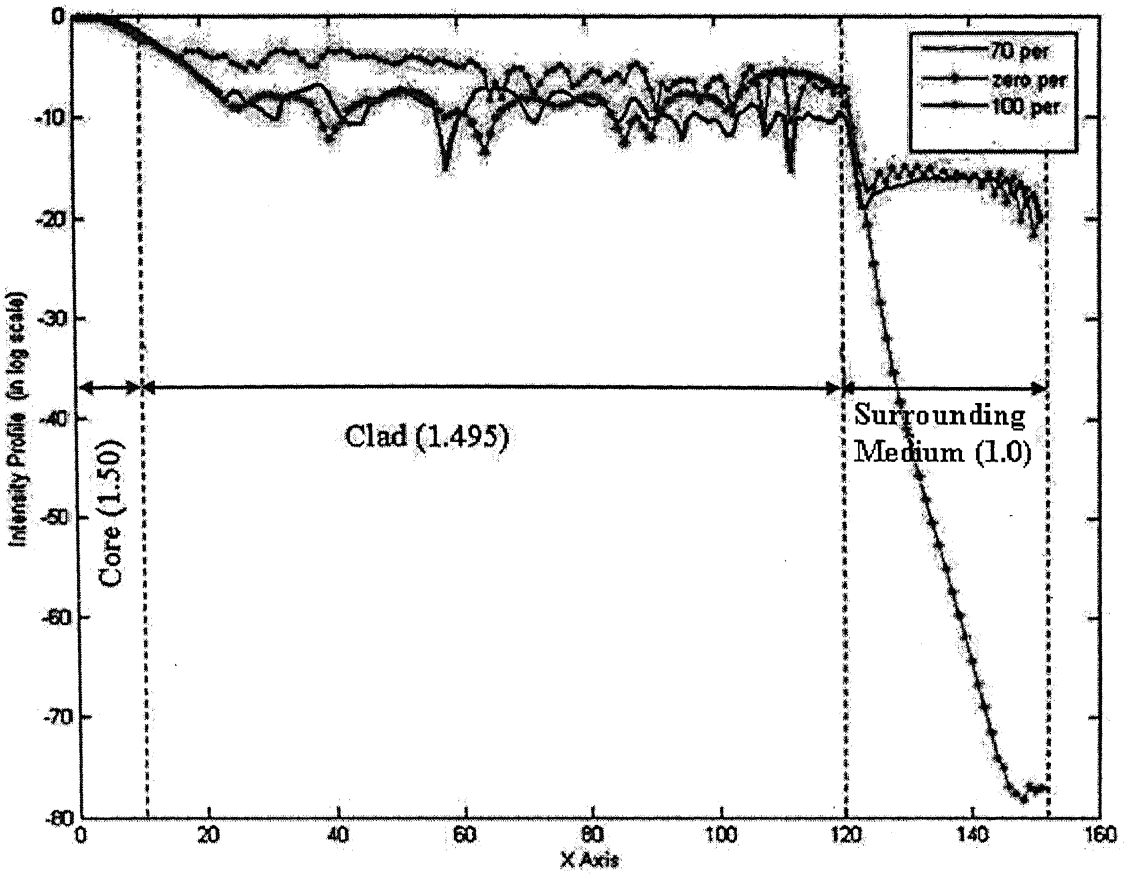


Figure 4.15 Intensity Profile for different Percentage of cut in cladding

4.5.2 Effect of Refractive Index on Output Power

Now we will discuss the effect of refractive Index on the output Power. As shown in the Figure (4.16) as we increase the refractive index of surrounding medium to the value up to cladding refractive index, the output power decreases because of decrease in the total internal reflection angle an so more power will go to the surrounding medium.

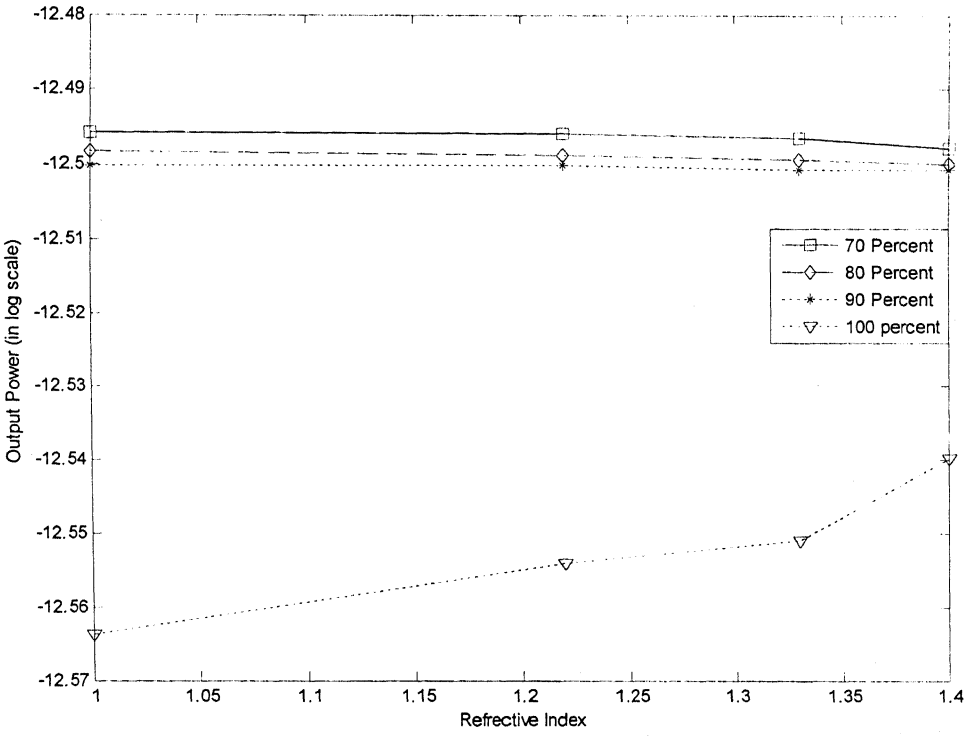


Figure 4.16 Effect of Refractive index (less than core) on the output power for different percentage of cladding removed structure

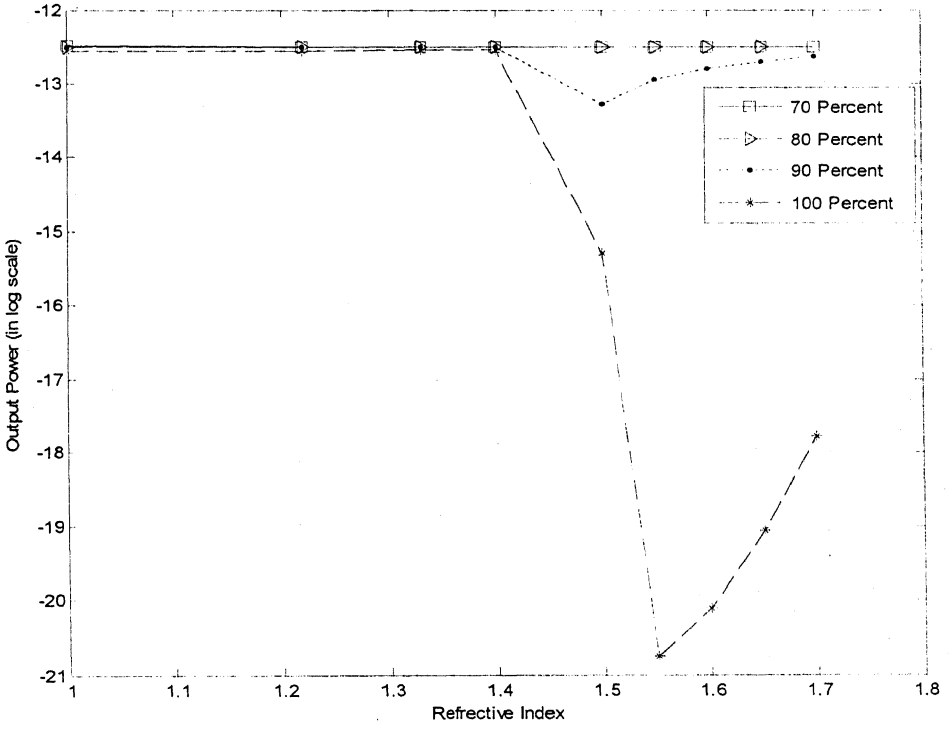


Figure 4.17 Effect of Refractive index on the output power for different percentage of cladding removed structure

Numerical Results shown in figure 4.16 also matches with practical results [22]. Now we will see the effect of refractive index more than the value of core refractive index (1.5) which is shown in Figure 4.17. From figure 4.19 we can see the combined effect of cross sectional cut and change in the refractive index. In each case of increase in the cut of cladding as well as the increase in refractive index, the output power becomes insensitive to the increase in the refractive index .

4.6 Optical Sensor

The new structure figure 4.18 is proposed here. In this structure two identical flat fibers are taken. Each flat fiber is allowing only single mode .They are separated 5um from each other. The 100 percent cross sectional cladding is removed upto 1cm from 1cm of start of launching the power in fiber. Figure 4.23 shows that as we increase the refractive index of surrounding material the power is coupling to other waveguide . It also tells that when the refractive index of surrounding material is approaching the value of core refractive index (1.5) then power is more coupling in the surrounding medium and other waveguide. Figure 4.19 and figure 4.20 shows the intensity profile at refractive index of surrounding is less than 1.5 and Figure 4.21 and figure 4.22 shows the intensity profile at refractive index of surrounding is 1.5. The sensitivity of this fiber with refractive index is shown in figure 4.23 . so Figure 4.23 can be used for measurement of optical properties of surrounding material like refractive index.

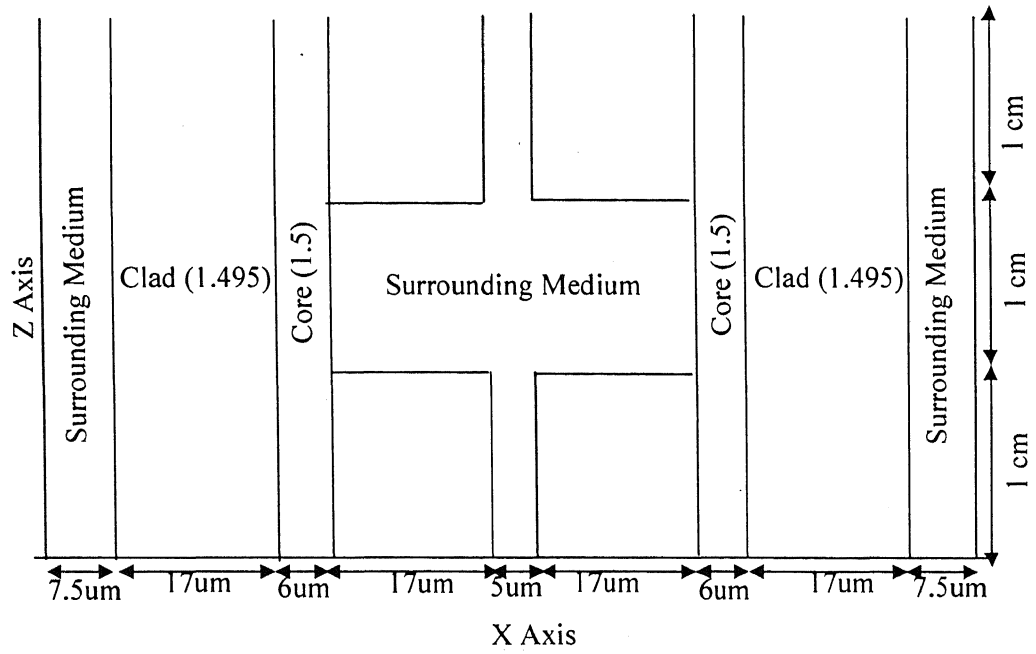


Figure 4.18 Structure Of Optical Sensor

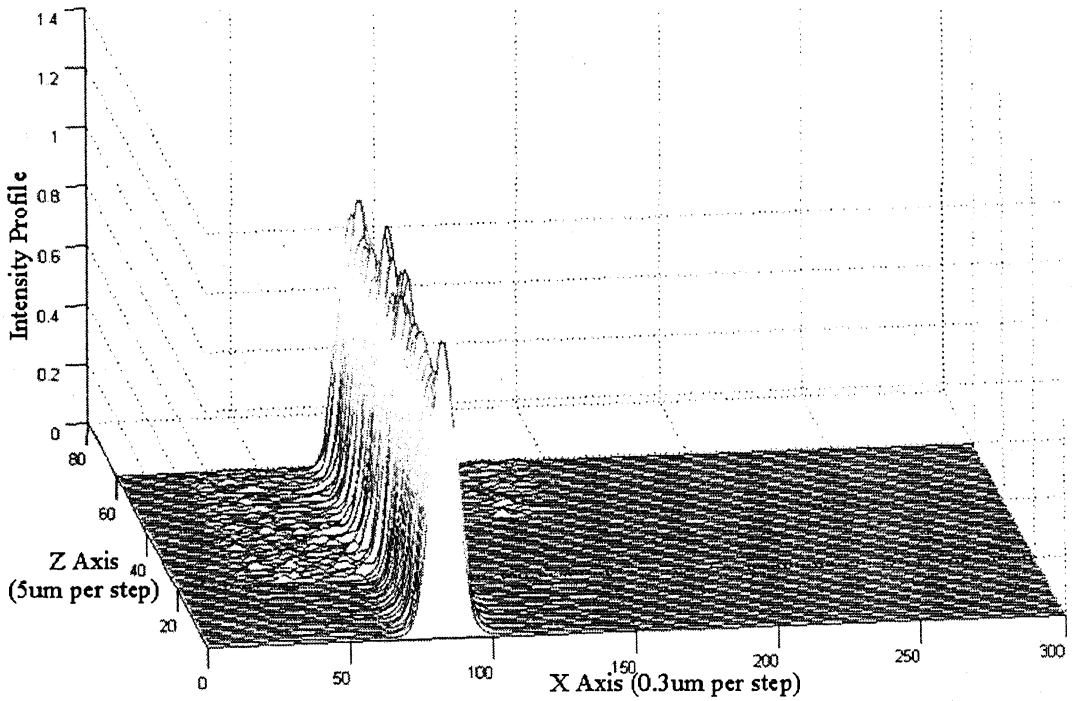


Figure 4.19 Intensity Profile for Surrounding Refractive Index at 1.44

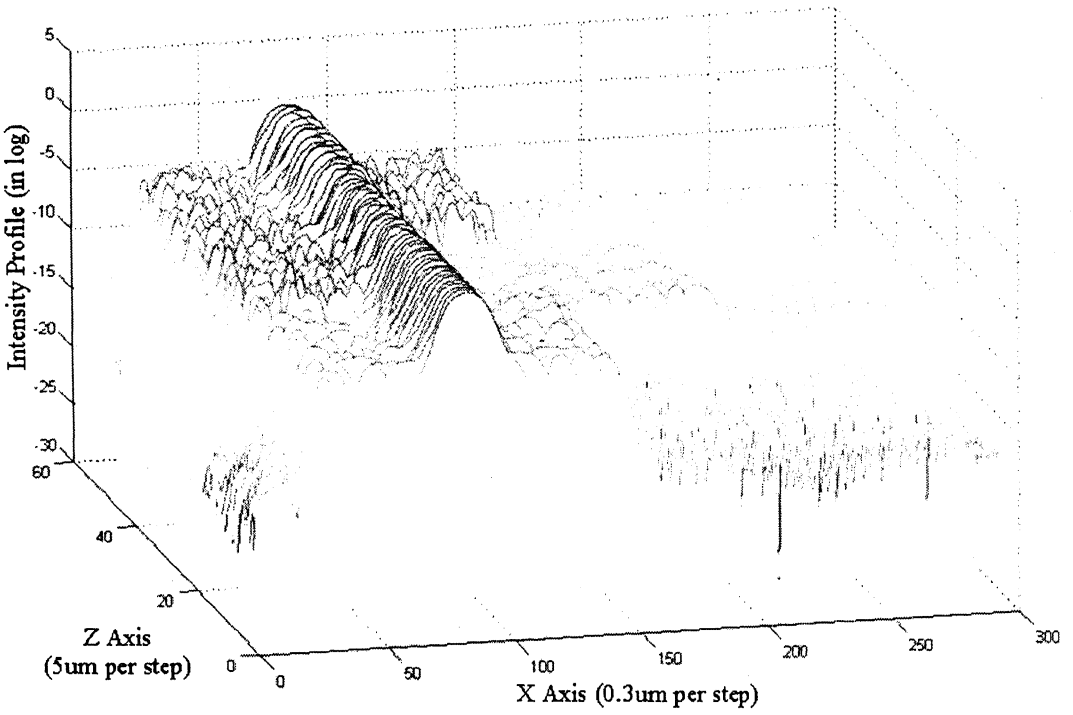


Figure 4.20 Intensity Profile for Surrounding Refractive Index at 1.44

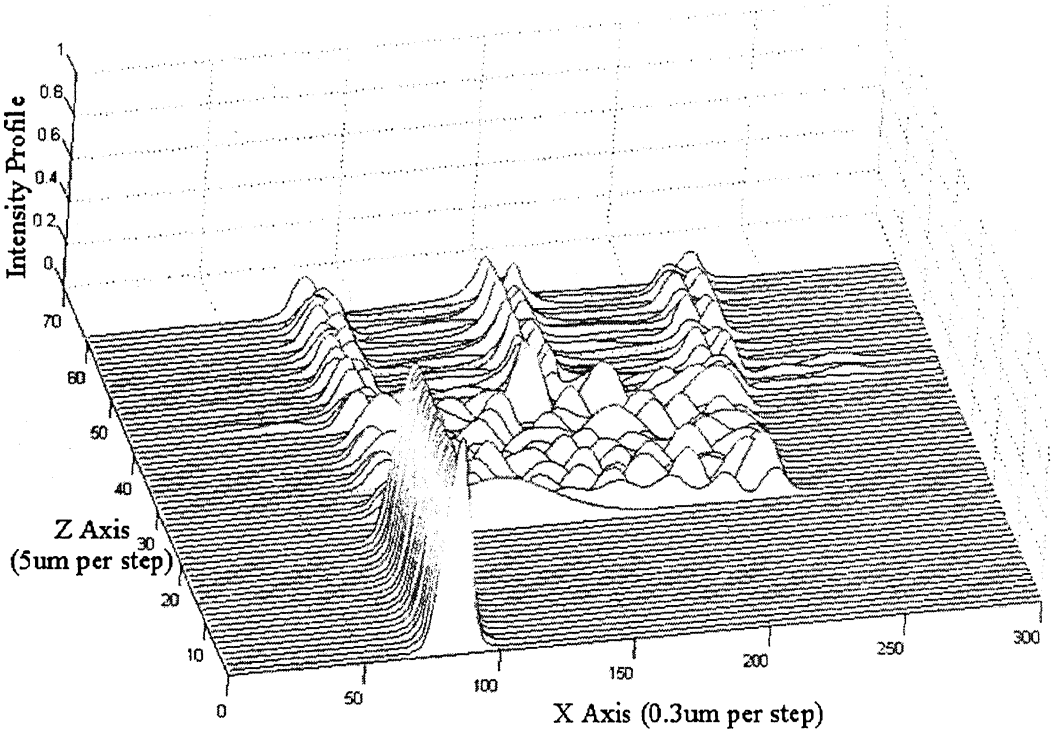


Figure 4.21 Intensity Profile for Surrounding Refractive Index at 1.50

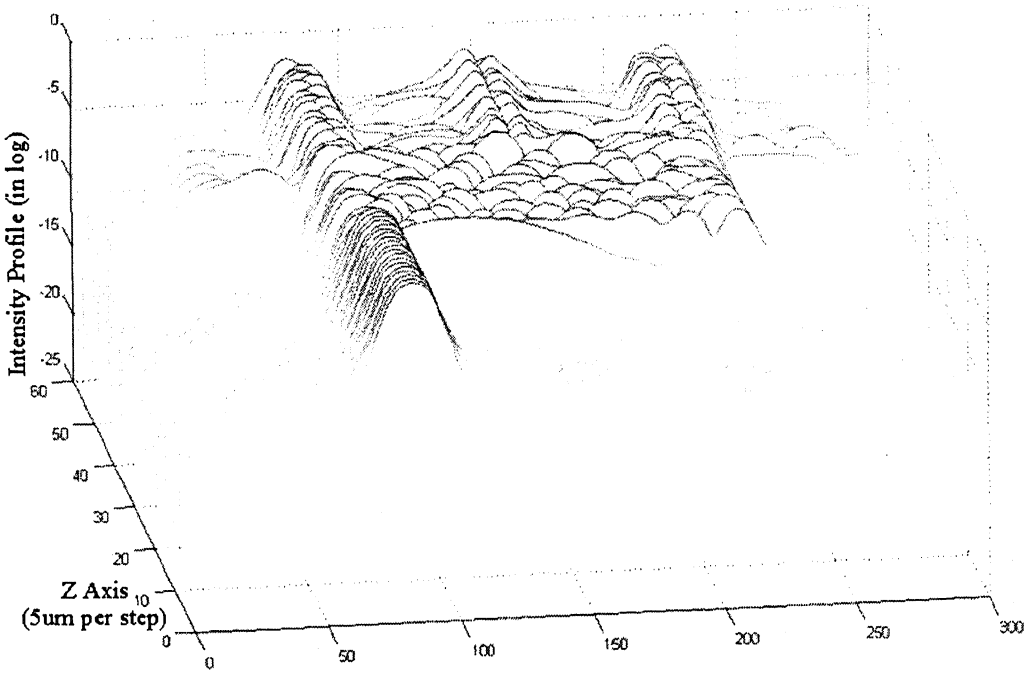


Figure 4.22 Intensity Profile for Surrounding Refractive Index at 1.50

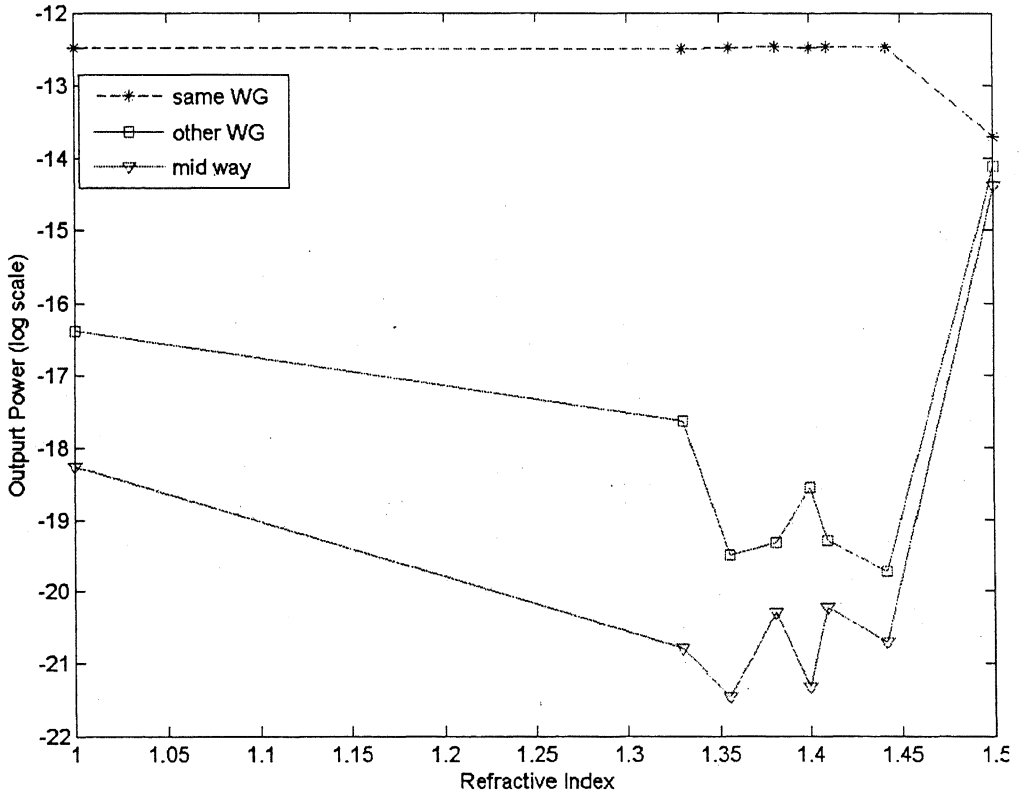


Figure 4.23 Effect of Refractive Index on Output Power

4.7 Effect of Strip

As fiber sensor is placed in liquid. Then liquid effects the power following in the fiber. Now it is assumed that liquid is not reacting with fiber so that no chemical change is coming in fiber or in the surrounding liquid. But if we put this sensor for more time in the liquid then small strip of layer is formed besides the fiber. This small strip affects the power flowing in the fiber. Here I have analyzed the effect of strip on the output power. I have taken strip of width 1um on both side of core at 100 percent clad removed section. Water is taken as surrounding material. Without any strip we are getting the output power 3.5414e-006 watt. Now by using strip we can see from figure 4.25 that the output power is greater when refractive index of strip is near the refractive index of core. Table 4.2 and Figure 4.25 gives the output power at different refractive index of strip. Figure 4.24 is shows the structure used for analysis of strip

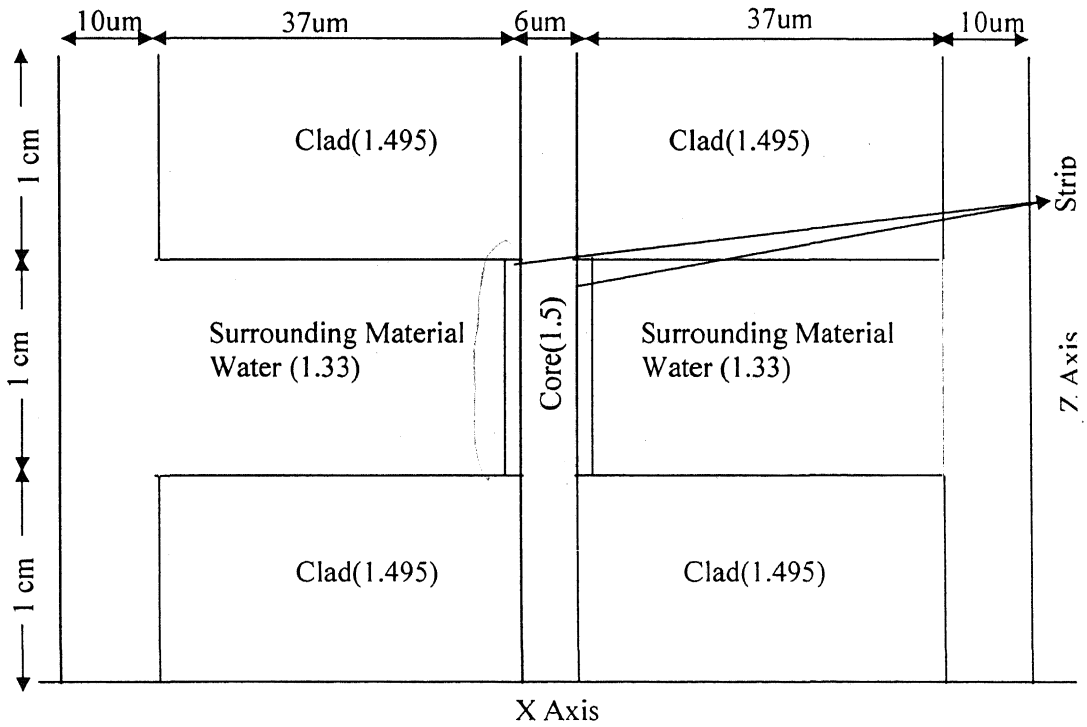


Figure 4.24 Structure with 1um strip on both side of core

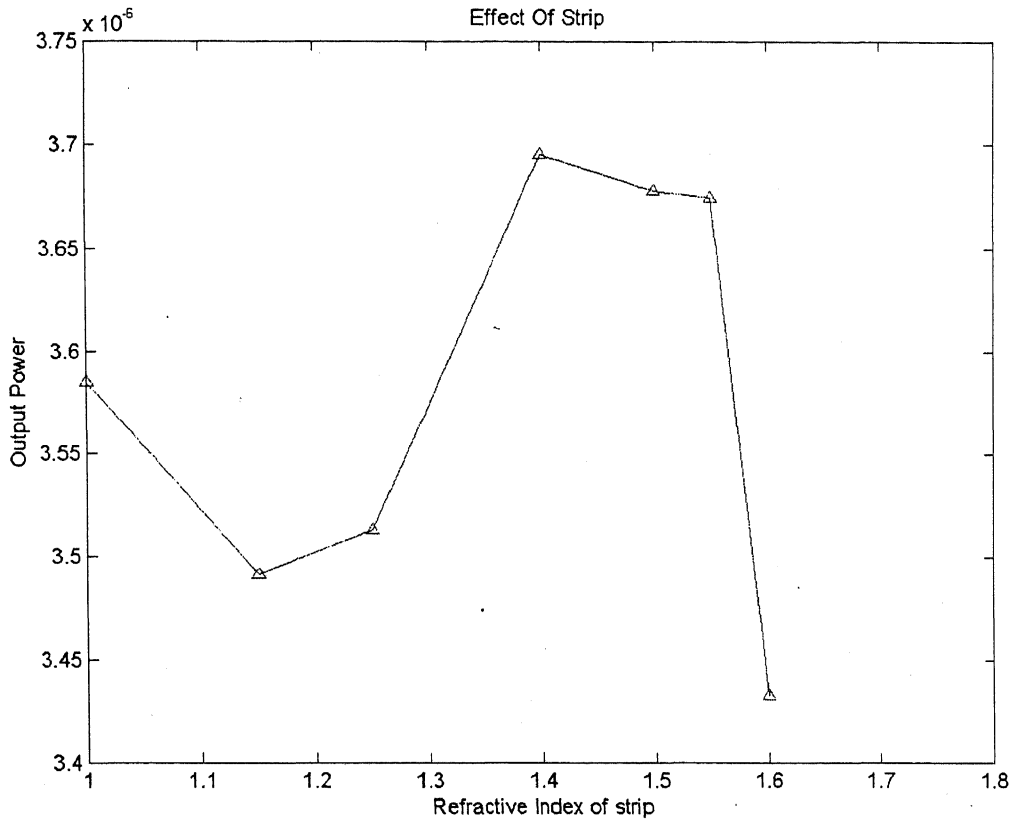


Figure 4.25 Effect of Strip on Output Power with Surrounding Refractive Index

RI (Surr. Medium)	Output Power(w) (with Strip)	Output Power(w) (No strip)
1.000	3.585e006	
1.330	3.492e-006	
1.400	3.513e-006	
1.450	3.695e-006	3.5414e-006
1.500	3.678e-006	
1.550	3.674e-006	
1.600	3.433e-006	

Table 4.2 Effect of strip Refractive Index on Output Power

4.8 Effect of Roughness in cladding Removal

Uptill now we have seen the effect of pure refractive index of surrounding material on the propagation of optical signal. We have also seen the effect of cladding removal. In real sensors when cladding is etched by enchants then surface is not perfectly flat etch. This roughness may effect the propagation of wave. In this section effect of roughness is analyzed. I have taken the sinusoidal perturbation at the core surface. The period of grating is equal to wavelength of propagation of optical signal. The structure used for the analyses of rough surface is shown in figure 4.26.

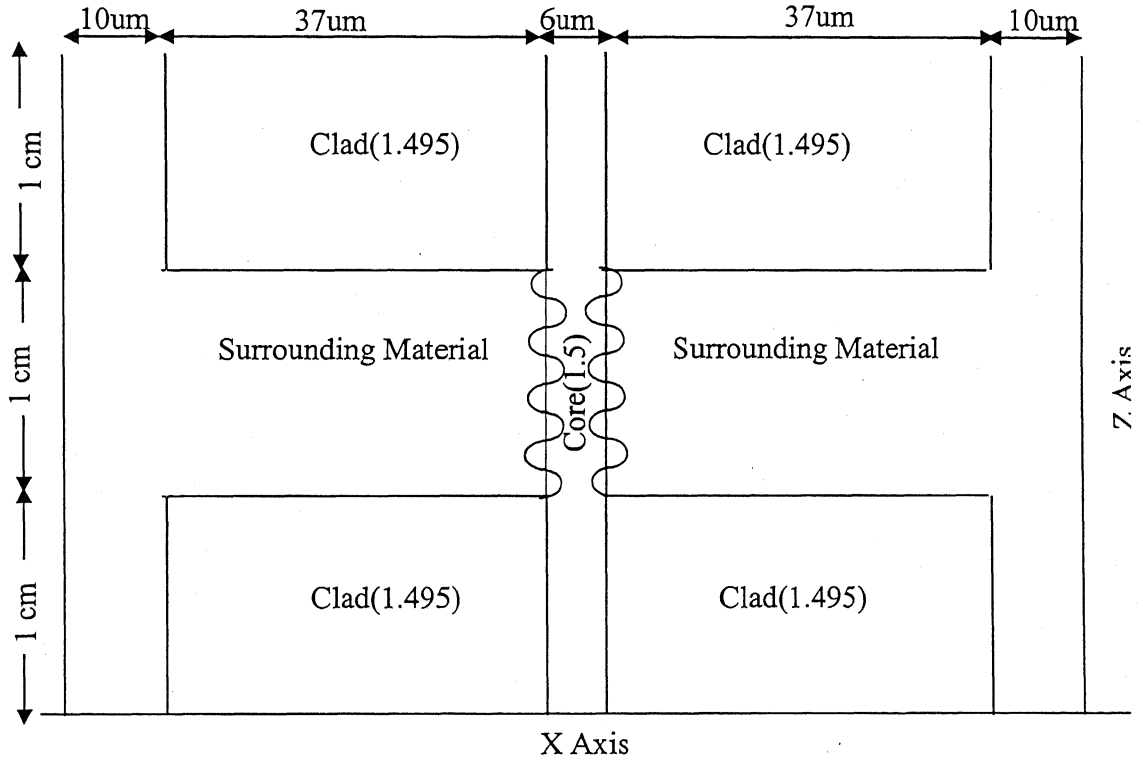


Figure 4.26 Waveguide structure with roughness due to cladding removal

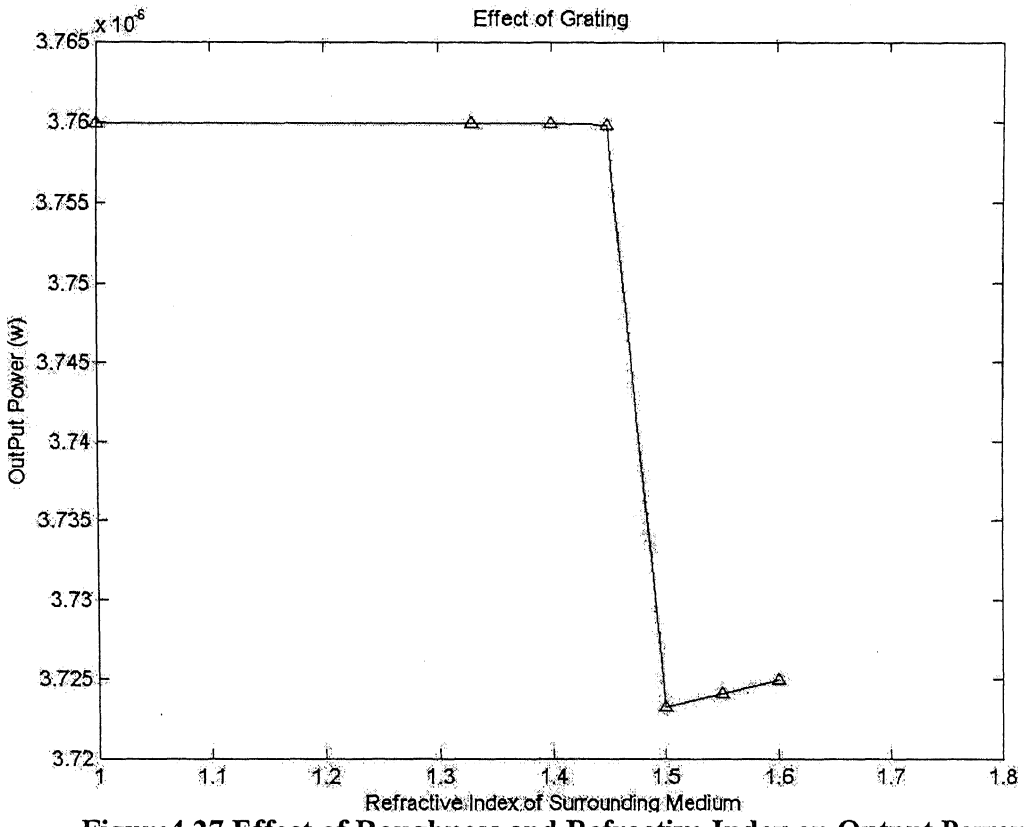


Figure4.27 Effect of Roughness and Refractive Index on Output Power

RI (Surr. Medium)	Output Power(w) (with Grating)	Output Power(w) (with flat surface)
1.000	3.760e-006	3.497e-006
1.330	3.760e-006	3.541e-006
1.400	3.760e-006	3.582e-006
1.450	3.760e-006	3.599e-006
1.500	3.723e-006	2.287e-007
1.550	3.724e-006	9.685e-010
1.600	3.725e-006	1.847e-009

Table 4.3 Effect of Roughness and Refractive Index on Output Power

Figure 4.27 shows the output power variation with roughness with different Refractive Index. Table 4.3 compares the output power with grating and without gratings for different refractive index of surrounding material. Table 4.3 shows that roughness at cladding is working as a grating which is trying to reduce the power leakage at the surrounding medium. This effect is clearly seen when the refractive

index of surrounding material (table 4.3) is increased above core refractive index. Here we are using fiber structure for single mode Propagation. Which signifies that we are using only one wavelength for propagation. Roughness is working as grating which is reflecting leaking power to the core. Using such type of fiber with grating we can reduce the width of fiber with removing extra cladding and surrounding medium. Such Type of fiber can help to reduce the area of integrated chip

CHAPTER 5

CONCLUSIONS AND SUGGESTIONS FOR FUTURE WORK

The aim of this thesis is to develop the numerical code using Finite Difference Beam Propagation Method. In this work a detailed analysis of Numerical Method FDBPM is presented. FDBPM is applied to a perturbed slab waveguide structure and effect of cladding removal and effect of refractive index is analyzed. The results are concluded as follows:

- An numerical method using FDBPM is developed for analysis of perturbed slab structures. Numerical code is also verified for free space Gaussian propagation and single mode slab waveguide structure

In the Perturbed slab waveguide we get the following results

- As the cross sectional cut percentage of the cladding increases the total output power of the core and the cladding is decreases.

- On increasing the refractive index of the surrounding Medium to the value up to the cladding refractive index the output power decreases.

- The combined effect of cross sectional cut of the cladding and change in the refractive index was observed with the increase of the cut of the cladding the output power become insensitive to the increase of the surrounding Medium refractive index

- The effect of strip besides the core is also observed as the refractive index of strip was near the core then output power is more than the without strip power.

5.1 SUGGESTIONS FOR FUTURE WORKS

- Accuracy of FDBPM can be increased by Appling the Wide angle Approximation and second order Transparent Boundary Condition.

- The result obtained by using this method can be validated with the experimental data.

- In our work we consider only propagation of Gaussian beam through a single slab waveguide structure. This work can be extended to array of waveguide structure analysis.

- In our estimation we assumed for the propagation of Gaussian beam has slowly varying envelop. It is helping to take large step size. It will be help full for saving the memory space as well as time of computation. It can also be extended for fast varying envelop to get more accuracy.

REFERENCES

1. M. S. Stern, "Semivectorial Polarized Finite Difference Method for Optical Waveguides with Arbitrary Index Profiles", Inst. Elec. Eng. Proc. J., Vol. 135, 988, pp 56-63.
2. K. Kawano and T Kitoh, " Introduction to Optical Waveguide Analysis", John Wiley & Sons Inc, 2001.
3. Pao-Lo Liu, S L Yang and D M Yuan, "The Semivectorial Beam Propagation Method", IEEE J. Quantum Electron., Vol. 29, No. 4, 1993, pp. 1205 – 1211.
4. http://www.nottingham.ac.uk/ggiemr/downloads/scg_chapter
5. http://www.nottingham.ac.uk/ggiemr/downloads/NT_chapter3.pdf.
6. Feit M.D. and Fleck J.A., "Light propagation in graded-index optical fibers", Applied Optics, Vol. 17, No. 24,1978, pp. 3990-3996.
7. Y. Chung, N. Dagli: "An Assessment of Finite Difference Beam Propagation Method"; IEEE J. Quantum Electron. Vol. 26 No. 8,1990, pp1335-1339.
8. Cheng D.K.," Field and Wave Electromagnetics", Second Edition, Pearson education, Inc., 2003.
9. Hecht E, "Optics" Fourth Edition, Pearson education, inc., 2003.
10. D. Yevick, "A guide to electric field propagation techniques for guided-wave optics," Opt. Quantum Electron., vol. 26, 1994, pp. S185–S197.
11. G. R. Hadley, "Transparent Boundary Condition for beam Propagation", Opt. Letters, Vol.16, No. 9, 1991, pp 624-626.
12. Jones W B, " Introduction to Optical Fiber Communication Systems", Holt, Rinehart and Winston, Inc 2000

13. Marcuse D.," Theory Of Dielectric Optical Waveguides", Academic Press,1974

14. Rsoft inc, http://www.rsoftdesign.com/

15. J.W. strohbehn "*Topics in Applied Physics*",vol.25,Springer-Verlag ,Berlin Heidelberg New York.

16. B.E.A. Saleh and M.C. Teich. "*Fundamentals of Photonics*", John Wiley & sons, inc., New York

17. Durana G, 'Dependence of bending losses on cladding thickness in plastic optical fibers', Applied Optics, Vol. 42, 997-1002, 2003

18. Mode scrambling and filtering, www.newport.com

19. Removal of cladding process, TECS, 3M company, www.3m.com

20. Merchant D C, 'Chemical tapering of polymer optical fiber', Sensor and Actuators, Vol. 76, 365-371, Nov. 1998

21. Asundi A, 'Determination of bacterial activity by use of an evanescent wave fiber optics sensor', Applied Optics, Vol. 41, 7334-7338, Dec 2002.

22. Bartlett R J, 'Automation and dynamic characterization of light intensity with applications to tapered plastic optical fiber', Applied Optics, Vol. 5, S51-S58, April 2003.